DECOMPOSITION ALGORITHMS FOR

MULTI-AREA POWER SYSTEM ANALYSIS

A Dissertation

by

LIANG MIN

Submitted to the Office of Graduate Studies of
Texas A&M University
in partial fulfillment of the requirements for the degree of

DOCTOR OF PHILOSOPHY

May 2007

Major Subject: Electrical Engineering

DECOMPOSITION ALGORITHMS FOR

MULTI-AREA POWER SYSTEM ANALYSIS

A Dissertation

by

LIANG MIN

Submitted to the Office of Graduate Studies of
Texas A&M University
in partial fulfillment of the requirements for the degree of

DOCTOR OF PHILOSOPHY

Approved by:

Chair of Committee,   Ali Abur
Committee Members,   Chanan Singh
                                    Peng Li
                                    Salih Yurttas
Head of Department,   Costas N. Georghiades

May 2007

Major Subject: Electrical Engineering

ABSTRACT

Decomposition Algorithms for Multi-area Power System Analysis. (May 2007)

Liang Min, B.S., Tianjin University, China;

M.S., Tianjin University, China

Chair of Advisory Committee: Dr. Ali Abur

A power system with multiple interconnected areas needs to be operated coordinately for the purposes of the system reliability and economic operation, although each area has its own ISO under the market environment. In consolidation of different areas under a common grid coordinator, analysis of a power system becomes more computationally demanding. Furthermore, the analysis becomes more challenging because each area cannot obtain the network operating or economic data of other areas.

This dissertation investigates decomposition algorithms for multi-area power system transfer capability analysis and economic dispatch analysis. All of the proposed algorithms assume that areas do not share their network operating and economic information among themselves, while they are willing to cooperate via a central coordinator for system wide analyses.

The first proposed algorithm is based on power transfer distribution factors (PTDFs). A quadratic approximation, developed for the nonlinear PTDFs, is used to update tie-line power flows calculated by Repeated Power Flow (RPF). These tie-line power flows are then treated as injections in the TTC calculation of each area, as the central entity coordinates these results to determine the final system-wide TTC value.

The second proposed algorithm is based on REI-type network equivalents. It uses the Continuation Power Flow (CPF) as the computational tool and, thus, the problem

of voltage stability is considered in TTC studies. Each area uses REI equivalents of external areas to compute its TTC via the CPF. The choice and updating procedure for the continuation parameter employed by the CPF is implemented in a distributed but coordinated manner.

The third proposed algorithm is based on inexact penalty functions. The traditional OPF is treated as the optimization problems with global variables. Quadratic penalty functions are used to relax the compatible constraints between the global variables and the local variables. The solution is proposed to be implemented by using a two-level computational architecture.

All of the proposed algorithms are verified by numerical comparisons between the integrated and proposed decomposition algorithms. The proposed algorithms lead to potential gains in the computational efficiency with limited data exchanges among areas.

To My Wife and Parents

ACKNOWLEDGMENTS

I would like to express gratitude to my advisor, Professor Ali Abur for his guidance, advice, and enthusiastic support during my doctoral studies. His profound knowledge of power systems, illuminating discussions and sharp comments to my ideas and papers encouraged me to continuously enhance this research. His thoughts will have a long-lasting influence on me.

Besides my advisor, I would like to thank the rest of my dissertation committee: Professor Chanan Singh, Professor Peng Li, and Professor Salih Yurttas for their precious time and support. Financial support for this research was provided by the National Science Foundation Grant No. ECS- 0400760.

My appreciation also goes to my office mates (Jian Chen, Jun Zhu, Bei Xu, Liang Zhao, C.Y. Evrenosoglu), who have provided me the most exciting working environment.

I would like to thank Dr. Stephen Lee and Dr. Pei Zhang at EPRI for providing me a nine-month internship during my doctoral studies. This internship made my doctoral time an enriching experience in both a professional and a personal perspective.

Family is the most important part of my life. I would like to thank my parents for their inspiration and unconditional love that have made me both success and happiness. I am especially grateful to my dear wife, Ying Lu, for her tireless support, encouragement and sacrifice.

TABLE OF CONTENTS

LIST OF TABLES

LIST OF FIGURES

FIGURE   Page

CHAPTER I

INTRODUCTION

An interconnected electric transmission grid inherently requires coordination of its use. In large networks, there may be multiple control areas with system operators responsible for different areas. Inevitably the multiple operators must have some procedure for exchanging information and making decisions that affect the patterns of use across grid.

With the introduction of competition in the utility industry, it is possible for customers to buy the less expensive electrical energy from remote location. System operators face the need to monitor and coordinate power transactions taking place over long distances in different areas. There are two questions related to the multi-area power system analysis:

(1) How much power can be transferred from the specific seller to the specific buyer?

(2) What is the maximum social benefit for all market participants?

In 1996, the North American Electric Reliability Council (NERC) now as Electric Reliability Organization (ERO) developed a framework for the determination of transfer capability and stated guidelines and standards for its implementation [1]. According to NERC's definition, total transfer capability (TTC) indicates the amount of power that can be transferred between two buses (or groups of buses) in the system in a reliable manner in a given time frame [1,2]. In other words, it is the largest flow in the selected interface for which there are no thermal overloads, voltage limit violations or total voltage collapse and/or any other system security problems. Usually,

---

This dissertation follows the style of *IEEE Transactions on Power Systems.*

TTCs evaluate by the ISO and power flow analysis is used to ensure that physical limits will not be violated for credible contingencies per system reliability criteria. The security of the system is assessed by monitoring a group of system elements that form the monitored elements set (lines, transformers, buses). Contingencies to be tested for violations are specified in the contingency set. This set may include single element contingency, i.e., loss of a line, generator, or transformer, or common mode contingencies, which include specific actions associated with certain outages. The single direction TTC study is completed with the identification of the transfer capability sequence, which includes an ordered set of capability for different transfer levels in the same direction. When the TTC study involves multiples transfer direction over the base case, the effect of simultaneous transfers should be considered in the study. NERC entrusted the security coordinators the responsibility to calculated and post transfer capability information. Usually, ISO will calculate and post transfer capability for inner Control Areas and the external Control Area Interfaces. Individual Transmission Providers will post transfer capability for their individual system. Marketers and transmission provides use those numbers on a daily basis to make decisions about the size(megawatt quantity,) direction, and price of transmission services, making the transfer capability numbers a key input to strategic operation.

Maintaining system security while maximizing social benefit for all market participants is a major ISO concern. In this context, there is a need to include suitable security constraints within the whole market pricing mechanism, so that the correct market signals can be sent to all market participants while operating the system within reasonable security margins. The FERC adopted the following definition of Security Constrained Economic Dispatch (SCED): the operation of generation facilities to produce energy at the lowest cost to reliably serve consumers, recognizing any operational limits of generation and transmission facilities [3]. The use of a regional,

security-constrained economic dispatch has produced lower prices and enhanced reliability in every region where it has been instituted. In general, a regional economic dispatch should inevitably result in lower prices because it enables system operators to turn to the lowest cost combination of resources to meet system needs, consistent with reliability. On a longer horizon, security-constrained economic dispatch provides effective financial signals and incentives for locating new generation and transmission facilities, which provides further cost savings to energy consumers.

Basically two approaches are used in TTC calculation. One is based on dc load flow which calculates power transfer distribution factors (PTDF) to determine the transfer capabilities of the power networks [4–6]. The fact that distribution factors are easy to calculate and can give quick, rough figures of TTC made them attractive. Since those factors are based on dc load flow ignoring voltage and reactive power effects as well as system nonlinearity, they might lead to unacceptable error especially in a stressed system with insufficient reactive power support and voltage control. Still PTDF can be used to update TTC in some systems where voltage problems are not pronounced [4]. These limitations of using DC load flow method in computing TTC can be avoided by using the Repeated Power Flow (RPF) [7].

The other approach for TTC calculation is the continuation power flow (CPF) algorithms, which can trace the power flow solution curve, starting at a base load, leading to the steady state voltage stability limit or the critical maximum loading point of the system [8–11]. They overcome the singularity of the Jacobian matrix near the saddle-node bifurcation point, or the critical point. Undoubtedly CPF is an important step further as compared with the dc load flow based approach because it takes system nonlinearity and voltage-reactive power aspects into consideration. However, to increase a certain power transfer, CPF uses a common loading factor for a specific cluster of generator(s) and load(s), which might lead to a conservative TTC

value since the optimal distribution of generation and loading is ignored. Besides the system reactive power optimization and voltage control are usually not considered in CPF, which might have significant impacts on system transfer capability.

Optimal power flow (OPF) problem has been investigated extensively in the past three decades [12, 13]. OPF techniques are quite mature and have found widespread applications in TTC studies [14, 15] and economic dispatch [13]. OPF methods can also play a crucial role in the current deregulated environment as it has the potential of distributing the resources optimally thus yielding considerable economic benefits to both power suppliers and customers. Furthermore, OPF can model the system constraints including ac load flow equations, transmission line thermal limits and voltage limits in both TTC and economic dispatch studies.

In the emerging competitive environment, TTC and economic dispatch are very important functions of any independent system operator (ISO), which is required to ensure the delivery of all the transactions without any violation on the operating limits of a transmission system. A system with multiple interconnected regions (or control areas) still needs to be operated coordinately for the purposes of the system reliability and economic operation, although each region (area) has its own ISO under the market environment. FERC Order 2000 has mandated the formation of Regional Transmission Organization (RTO), which will accelerate interregional transaction and increase the burden of interregional transmission [16]. The Association of European Transmission System Operators (ETSO), founded in July 1999, has been investigating congestion management methods for cross-border transmission between European countries [17]. In consolidation of different regions (or control areas) under a common grid coordinator, TTC and economic dispatch studies become computationally demanding. Furthermore, these studies become more challenging for the coordinated interregional planning across multi-area interconnected power system. Since each re-

gional ISO (or control areas) cannot obtain the network operating or economic data of other regions (or areas), one of the main difficulties to meet the requirement presented in [16,17] is how to implement the interregional planning coordinately without a huge amount of information exchange between regions.

The objective of this dissertation is to investigate and propose methods to analyze multi-area interconnected power system. The dissertation will present three new system decomposition frameworks. Based on these decomposition frameworks, decentralized versions of prevalent power flow methods: RPF, CPF, OPF will be developed in order to analyze multi-area power system. The dissertation will also identify the required amount of information exchange and coordination across multiple areas.

Chapter II presents a decomposition method based on Power Transfer Distribution Factors (PTDFs) for multi-area TTC computation. A quadratic approximation is developed for the nonlinear PTDFs by using the Taylor series expansion. This approximation is used to update PTDFs, which are then used to calculate nonlinear TTC in each control area while a central entity coordinates these results to determine the final system-wide TTC value. Due to the the characterizes of PTDFs, the proposed method in this chapter is limited to solve the multi-area TTC problem without the consideration of voltage stability and contingencies. The developed procedure is successfully applied to calculate the single TTC and simultaneous TTC for the IEEE 118 bus test system.

Chapter III initiates a network decomposition method based on REI-type network equivalents for multi-area TTC computation. The proposed method overcomes the limitations of PTDF-based decomposition method. The computation in this chapter takes into account the limits on the line flows, bus voltage magnitude, generator reactive power, voltage stability as well as the loss of line contingencies. Each area uses REI equivalents of external areas to compute its TTC via the Continuation

Power Flow (CPF). The choice and updating procedure for the continuation parameter employed by the CPF is implemented in a distributed but coordinated manner. The proposed method leads to potential gains in the computational efficiency with limited data exchanges between areas. The developed procedure is successfully applied to the 3 area IEEE 118 bus test system. Numerical comparisons between the integrated and the proposed multi-area solutions are presented for validation.

Chapter IV presents a decomposition method for multi-area Optimal Power Flow (OPF) problem. Applying this method to the multi-area OPF problem will yield an optimal coordinated but decentralized solution. The proposed method is efficient in solving the OPF problem with limited data exchange between areas. The developed method is successfully implemented and tested using the 3 area IEEE 30 bus test system. Numerical results comparing the solutions obtained by the traditional and the proposed decentralized methods are presented for validation.

CHAPTER II

POWER TRANSFER DISTRIBUTION FACTORS BASED DECOMPOSITION
ALGORITHM

A. Introduction

Repeated Power Flow (RPF) is the most prevalent method for integrated system
TTC computation. DC-based load flow solution which calculates PTDFs to determine
the transfer capabilities of the power networks was reported in [4]. Since those factors
are based on DC load flow method ignoring voltage and reactive power effects as well
as system nonlinearity, they might lead to unacceptable errors, especially in a stressed
system with insufficient reactive power support and voltage control. These limitations
of using DC load flow method in computing TTC can be avoided by using the AC
RPF method [5]. Several commercially available software packages use RPF solution
to assess system security and transfer capability, such as DSA Power Tools [18] and
POM by V&R Energy, Inc [19].

Calculation of TTC by RPF method is commonly undertaken by the independent
system coordinator, which has access to the entire network model and its current
operating state. While the TTC calculation typically involves all contingencies and
stability limits, in this work only the line power flow and bus voltage limits will be
considered.

As the size of the systems grow due to the consolidation of different control areas
under a common grid coordinator, calculation of TTC becomes more challenging. It
requires collection of network data from all control areas and solving a very large-
scale power flow problem considering all limits in all areas. One alternative method,
which is based on a two-level multi-area coordinated solution approach, is presented

recently [20]. The main idea is to distribute the computations into individual areas and then coordinate their solutions in order to reach the system-wide solution. The main objective is to compute a TTC value, which is very close to the TTC that would be calculated if the entire system information was available to a single central operator.

Such problem is a two-level decision problem, where each control area's TTC calculation is considered as low level and the central operator's coordination is considered as the high level. The algorithm, consisting of decomposition and coordination, leads to the hierarchical computational model.

Such hierarchical computational model can be solved by hierarchical optimization method [21]. In [22], Bender decomposition is used to calculate the ATC, where the base case security constraints are treated as the high level problem and the contingencies are handled as a series of low level problems.

An alternative method is repeated power flow. This is adopted in [20], where a two-layer multi-area linear TTC calculation algorithm by using linear PTDFs is proposed. Linear PTDFs are approximations of the first order sensitivities of the active power flows with respect to various variables [1, 2, 23]. An insightful characterization of PTDFs - their insensitivity to the system loadings under certain conditions - is discussed in [24]. In [25], a detailed analysis of the variation of PTDFs while maintaining the bus voltage magnitudes constant and a discussion of how PTDFs vary with loading in lossless power systems, are given. All of these approaches make the assumption of maintaining constant voltage magnitudes. In [26], numerical integration is used to calculate nonlinear allocation of quantities to transactions.

This chapter extends the previous work [20] and a quadratic approximation of the nonlinear PTDFs is developed by using the Taylor series expansion. This approach does not require any numerical integration, but just a single power flow solution.

Again, a hierarchical computation model is used. Here, the PTDFs are updated in order to accurately calculate the nonlinear TTC in each control area while a central operator coordinates these results to determine the final TTC value.

B. Assumptions and Formulation

It is assumed that each bus belongs to only one area, whereas a system branch is either inside an area or is connecting two areas (a tie line). The following definitions will be given first:

Ω	Set of all buses of the entire system,
Ω_k	Set of all buses of the area k,
ψ_k	Set of internal buses of the area k, excluding the slack bus,
λ_k	Set of boundary buses of the area k, excluding the slack bus,
σ	Set of all PQ buses of the entire system,
σ_k	Set of all PQ buses of the area k,
ϕ	Set of all lines of the entire system,
ϕ_k	Set of all internal lines of the area k,
γ_k	Set of all tie lines of the area k,
δ_k	Set of tie lines which are incident to boundary bus i.

1. Integrated System TTC Problem Formulation

TTC calculation requires the evaluation of transmission lines thermal limits, voltage magnitude limit, transient stability and voltage collapse limits. In this paper, we assume that system transient and steady state stability are not jeopardized and voltage limits are reached before the system reaches the nose point and loses voltage stability. Only the power flow limit and voltage magnitude limit will be considered.

Single transaction is considered in this chapter.

The problem is formulated in the form:

$$Max.J = f(x, \mu) \tag{2.1}$$

subject to

$$g(x, \mu) = 0 \tag{2.2}$$

$$h(x, \mu) \leq 0 \tag{2.3}$$

where μ and x are the control and state vectors respectively. g and h are system equality and inequality constraints.

Assuming TTC to be evaluated is between the sending bus I (Seller) and the receiving bus J (Buyer), detailed expressions of the objective function and constraints are formulated as:

$$Max.P_J^{TTC} \tag{2.4}$$

subject to

$$P_i - V_i \sum_{j \in \Omega} V_j (G_{ij} \cos \theta_{ij} + B_{ij} \sin \theta_{ij}) = 0 \quad i \in \Omega, i \neq I, J \tag{2.5}$$

$$P_J - P_J^{TTC} - V_J \sum_{j \in \Omega} V_j (G_{ij} \cos \theta_{ij} + B_{ij} \sin \theta_{ij}) = 0 \tag{2.6}$$

$$Q_i - V_i \sum_{j \in \Omega} V_j (G_{ij} \sin \theta_{ij} - B_{ij} \cos \theta_{ij}) = 0 \quad i \in \sigma \tag{2.7}$$

$$0 \leq |P_l| \leq P_l^{max} \quad l \in \Phi \tag{2.8}$$

$$V_{min} \leq V_i \leq V_i^{max} \quad i \in \Omega \tag{2.9}$$

where P_J^{TTC} is the TTC between the sending bus I and the receiving bus J; P_i and Q_i are net active and reactive power injection to bus i; $V_i \angle \theta_i$ is the voltage magnitude and angle respectively at bus i; $G_{ij} + jB_{ij}$ is the bus-admittance matrix element at
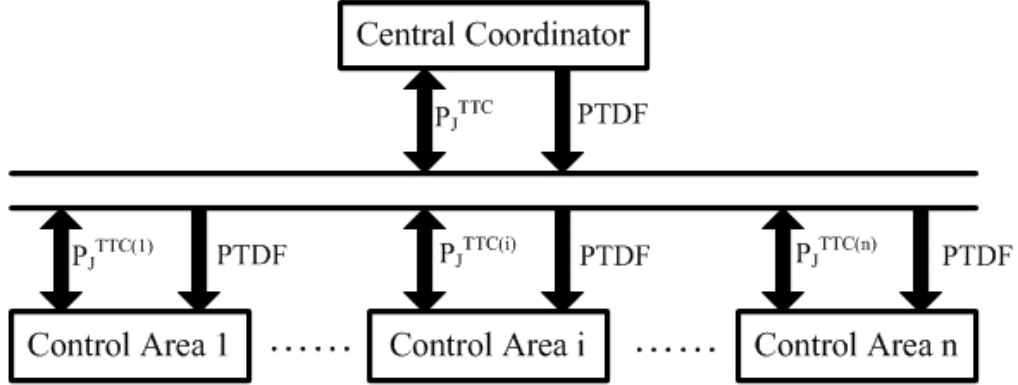
Fig. 1. Two-level multi-area TTC computational model.

row i and column j; P_l and P_l^{max} are the active power flow the upper limit of active power flow through the line l; V_i^{min} and V_i^{max} are lower and upper limits of voltage magnitude at bus i. (2.5-2.7)are the AC power flow equation; (2.8) is the branch power flow limit; (2.9) is the bus voltage magnitude limit. Note that the sending bus I is considered as the slack bus in the formulation.

2. Two-Level Multi-Area TTC Computational Mode

The two-level computational model of TTC calculation in a multi-area power system, which has n control areas, is shown in Fig. 1. Control areas do not necessarily share their network data with others. The central coordinator derives quadratic approximation of nonlinear PTDFs of all tie-lines of the entire system. Then, each control area using the approximation to update the PTDFs and solves its own TTC problem. Finally, the central operator coordinates the results from each control area and then determines the final TTC value between the specified buyers and sellers.

The control areas can belong to one of the following three categories:

1. A control area, which contains the sending bus;

2. A control area, which contains the receiving bus;

3. A control area, which contains neither.

If area k belongs to the first category, the sending bus will be automatically selected as the slack bus of the area. If area k belongs to the third category, the bus SL_k will be selected as the slack bus of the area. These two categories have the same TTC calculation problem formulation as:

$$Max.P_J^{TTC(k)} \tag{2.10}$$

subject to

$$P_i - V_i \sum_{j \in \Omega_k} V_j(G_{ij} \cos \theta_{ij} + B_{ij} \sin \theta_{ij}) = 0 \quad i \in \psi_k \tag{2.11}$$

$$Q_i - V_i \sum_{j \in \Omega_k} V_j(G_{ij} \sin \theta_{ij} - B_{ij} \cos \theta_{ij}) = 0 \quad i \in \sigma_k \tag{2.12}$$

$$P_i - \sum_{l \in \delta_i} \left(\int_{P_J^0}^{P_J^{TTC(k)}} PTDF_l(\mu)d\mu + P_l^0 \right) \\ - V_i \sum_{j \in \Omega_k} V_j(G_{ij} \cos \theta_{ij} + B_{ij} \sin \theta_{ij}) = 0 \quad l \in \delta_i, i \in \lambda_k \tag{2.13}$$

$$0 \le |P_l| \le P_l^{max} \quad l \in \Phi_k \tag{2.14}$$

$$0 \le \left| \int_{P_J^0}^{P_J^{TTC(k)}} PTDF_l(\mu)d\mu + P_l^0 \right| \le P_l^{max} \quad l \in \gamma_k \tag{2.15}$$

$$V_{min} \le V_i \le V_i^{max} \quad i \in \Omega_k \tag{2.16}$$

If area k belongs to the second category, the bus SL_k will be selected as the slack bus of the area. Then, the TTC calculation Problem in the area can be formulated as:

$$Max.P_J^{TTC(k)} \tag{2.17}$$

subject to

$$P_i - V_i \sum_{j \in \Omega_k} V_j (G_{ij} \cos \theta_{ij} + B_{ij} \sin \theta_{ij}) = 0 \quad i \in \psi_k, i \neq J \tag{2.18}$$

$$Q_i - V_i \sum_{j \in \Omega_k} V_j (G_{ij} \sin \theta_{ij} - B_{ij} \cos \theta_{ij}) = 0 \quad i \in \sigma_k \tag{2.19}$$

$$P_i - \sum_{l \in \delta_i} \left(\int_{P_J^0}^{P_J^{TTC(k)}} PTDF_l(\mu) d\mu + P_l^0 \right)$$

$$- V_i \sum_{j \in \Omega_k} V_j (G_{ij} \cos \theta_{ij} + B_{ij} \sin \theta_{ij}) = 0 \quad l \in \delta_i, i \in \lambda_k, i \neq J \tag{2.20}$$

$$P_J - P_J^{TTC(k)} - V_J \sum_{j \in \Omega_k} V_j (G_{ij} \cos \theta_{ij} + B_{ij} \sin \theta_{ij}) = 0 \tag{2.21}$$

$$0 \leq |P_l| \leq P_l^{max} \quad l \in \Phi_k \tag{2.22}$$

$$0 \leq \left| \int_{P_J^0}^{P_J^{TTC(k)}} PTDF_l(\mu) d\mu + P_l^0 \right| \leq P_l^{max} \quad l \in \gamma_k \tag{2.23}$$

$$V_{min} \leq V_i \leq V_i^{max} \quad i \in \Omega_k \tag{2.24}$$

where $P_J^{TTC(k)}$ is area k's TTC which is to be determined. P_l^0 and P_J^0 are the power flow through the line l and the injection of bus J at the initial operating condition. $PTDF_l$ is the Power Transfer Distribution Factor from the injection at bus J to flow on the tie line l, the injection at receiving bus J is the amount of transfer from the slack bus to bus J. In my approach, $PTDF_l$ need to be updated with the increase of the amount of transfer. (2.15) and (2.23) give the power flow limits of the tie lines.

C. Power Transfer Distribution Factors

1. Linear PTDFs

The linearity property of the DC power flow model can be used to find the injection amount that would contribute to a specific power flow. Consider a bus m and

a line joining buses j and k. Following Wood and Wollenberg [23], the coefficient of the linear relationship between the incremental amount of an injection and the incremental flow on a line is called the (incremental) power transfer distribution factor (PTDF).

The (incremental) PTDF from injection at bus m to flow over the transmission line connecting bus j and bus k is the sensitivity:

$$PTDF_{jk,m} = \frac{X_{jm} - X_{km}}{x_{jk}} \tag{2.25}$$

where x_{jk} is the reactance of the transmission line connecting bus j and bus k; X_{jm} is the element on the jth row and the mth column of the bus reactance matrix. For brevity, I call this sensitivity "the PTDF from m to line jk".

From the power flow point of view, a transaction is a specific amount of power that is injected into the system at one bus m by a generator and removed at another bus by a load n. In this case, then the PTDF from injection at bus m and withdrawal at bus n to flow on the line connecting bus j and bus k is the difference of sensitivities:

$$PTDF_{jk,mn} = PTDF_{jk,m} - PTDF_{jk,n} = \frac{X_{jm} - X_{km} - X_{jn} + X_{kn}}{x_{jk}} \tag{2.26}$$

where x_{jk} is the reactance of the transmission line connecting bus j and bus k; X_{jm} is the entry in the jth row and the mth column of the bus reactance matrix X. For brevity, I call this sensitivity "the PTDF from mn to line jk".

The change in line flow associated with a new transaction is then

$$\triangle P_{jk}^{New} = PTDF_{jk,mn} \cdot P_{mn}^{New} \tag{2.27}$$

where j and k are the buses at the ends of the line being monitored; m and n are the "from" and "to" buses for the proposed new transaction; P_{mn}^{New} is the new transaction

MW amount.

2. Nonlinear PTDFs

The linear PTDFs reviewed above depend on the topology of the electric power system only. While, in AC analysis, the PTDFs depend on not only the system topology but also the operating point. The evaluation of PTDFs at an operating point from the Jacobian of the power flow equations is also described in [23], section 13.3.

The active power flow from bus j to bus k is defined as:

$$P_{jk} = V_j^2 G_{jk} - V_j V_k (G_{jk} \cos \theta_{jk} + B_{jk} \sin \theta_{jk}) \tag{2.28}$$

We use the standard Newton Power Flow relationship between changes in state variables and changes in the power injection [23], so that:

$$
\begin{bmatrix} \dfrac{\partial P_{jk}}{\partial \theta_i} \\ \dfrac{\partial P_{jk}}{\partial V_i} \end{bmatrix} = \begin{bmatrix} \dfrac{\partial P_m}{\partial \theta_i} & \dfrac{\partial Q_m}{\partial \theta_i} \\ \dfrac{\partial P_m}{\partial V_i} & \dfrac{\partial Q_m}{\partial V_i} \end{bmatrix} \cdot \begin{bmatrix} \dfrac{\partial P_{jk}}{\partial P_m} \\ \dfrac{\partial P_{jk}}{\partial Q_m} \end{bmatrix} = [J^T] \cdot \begin{bmatrix} \dfrac{\partial P_{jk}}{\partial P_m} \\ \dfrac{\partial P_{jk}}{\partial Q_m} \end{bmatrix} \tag{2.29}
$$

Thus, the power transfer distribution factor from the injection at bus m to the power flow on the line jk can be expressed as:

$$
\begin{bmatrix} \dfrac{\partial P_{jk}}{\partial P_m} \\ \dfrac{\partial P_{jk}}{\partial Q_m} \end{bmatrix} = [J^T]^{-1} \cdot \begin{bmatrix} \dfrac{\partial P_{jk}}{\partial \theta_i} \\ \dfrac{\partial P_{jk}}{\partial V_i} \end{bmatrix} \tag{2.30}
$$

where the injection shift fact of the line connecting bus j with bus k with respect to a change in injection at bus m is, $PTDF_{jk,m} = \dfrac{\partial P_{jk}}{\partial P_m}$; In the right hand side of the equation, change in the active power flow of line jk with respect to changes in state

variables is determined as:

$$\frac{\partial P_{jk}}{\partial \theta_i} = \begin{cases} 0 & i \neq j, k \\ V_j V_k (G_{jk} \sin \theta_{jk} - B_{jk} \cos \theta_{jk}) & i = j \\ V_j V_k (-G_{jk} \sin \theta_{jk} + B_{jk} \cos \theta_{jk}) & i = k \end{cases} \tag{2.31}$$

$$\frac{\partial P_{jk}}{\partial V_i} = \begin{cases} 0 & i \neq j, k \\ 2V_j G_{jk} - V_k (G_{jk} \cos \theta_{jk} + B_{jk} \sin \theta_{jk}) & i = j \\ -V_j (G_{jk} \cos \theta_{jk} + B_{jk} \sin \theta_{jk}) & i = k \end{cases} \tag{2.32}$$

If a transaction involve a change in injection at bus m and a corresponding withdrawal at bus n, the nonlinear PTDF in AC system is also can be calculated by:

$$PTDF_{jk,mn} = PTDF_{jk,m} - PTDF_{jk,n} \tag{2.33}$$

where $PTDF_{jk,m}$ and $PTDF_{jk,n}$ can be calculated from (2.30). Note that the PTDF from slack bus to line jk, $PTDF_{jk,slack} \equiv 0$.

From (2.30), we can see that the PTDFs are functions of the operating point. If we just consider a single power transfer, where the operating point is a function of the injections, the PTDFs will also be functions of the transfer.

The power flow through the transmission line jk due to a new transaction P_{mn}^{New} can be expressed as:

$$P_j k = \int_0^{P_{mn}^{New}} PTDF_{jk,mn}(\mu) d\mu + P_{jk}^0 \tag{2.34}$$

where P_{jk}^0 is the power flow through the line jk at the initial operating condition.

3. Behavior of PTDFs Near Static Collapse

In this section, the behavior of operating point dependent active power distribution factors is analyzed. At a given operating point driven by a transfer, the distribution factor is computed exactly as (2.33) where all the terms are operating point dependent sensitivities and the sensitivities with respect to the system state variables can be explicitly obtained from (2.30). Since the Jacobian becomes singular at collapse, the sensitivities to the parameter in the previous expression diverge as the point of collapse is approached. Thus, it is expected that distribution factors in meshed system experience considerable changes close to collapse. I illustrate these changes in the numerical example of this chapter, which shows typical distribution factors across alternative parallel links for values of in the interval.

Therefore, PTDF based method is not suitable for the TTC computation considering voltage stability problem. In this chapter, the TTC computation just consider the thermal and voltage constraints and assume that the system satisfy the voltage stability condition.

4. Quadratic Approximation

It is hard to analytically formulate the relationship between the PTDFs and the injections, because the matrix $[J]$ and $\left[\frac{\partial P_{jk}}{\partial \theta_i}, \frac{\partial P_{jk}}{\partial V_i}\right]^T$ in (2.30) are both functions of injections. Thus, a second-order Talyor series expansion is used to approximate the PTDFs as below:

$$\frac{\partial P_{jk}}{\partial P_m} = \frac{\partial P_{jk}}{\partial P_m}|_{P_m=P_m^0} + (P_m - P_m^0)\frac{\partial^2 P_{jk}}{\partial P_m^2}|_{P_m=P_m^0} + \frac{1}{2}(P_m - P_m^0)^2\frac{\partial^3 P_{jk}}{\partial P_m^3}|_{P_m=P_m^0} \quad (2.35)$$

$$\frac{\partial P_{jk}}{\partial Q_m} = \frac{\partial P_{jk}}{\partial Q_m}|_{Q_m=Q_m^0} + (Q_m - Q_m^0)\frac{\partial^2 P_{jk}}{\partial Q_m^2}|_{Q_m=Q_m^0} + \frac{1}{2}(Q_m - Q_m^0)^2\frac{\partial^3 P_{jk}}{\partial Q_m^3}|_{Q_m=Q_m^0} \quad (2.36)$$

where (P_m^0, Q_m^0) is the injection at bus m at the initial operating point. The expressions of $\dfrac{\partial^2 P_{jk}}{\partial P_m^2}$, $\dfrac{\partial^2 P_{jk}}{\partial Q_m^2}$ and $\dfrac{\partial^3 P_{jk}}{\partial P_m^3}$, $\dfrac{\partial^3 P_{jk}}{\partial Q_m^3}$ are derived in the Appendix A.

The elements in the right side of (2.35) and (2.36) can be obtained at the initial operating condition except for the injection (P_i, Q_i). Thus, a quadratic formulation is derived to approximate the relationship between the PTDFs and injections by executing a single power flow at the initial operating condition.

D. Proposal Procedure

1. Central Coordinator

The central coordinator does not know the detail operating information of each area and just executes two functions:

1. Derive the quadratic approximation of PTDFs by executing a single power flow at initial operating condition;

2. Compare the values of P^{TTC} obtained from each control area and find the smallest one, and then determine the final TTC value between the specified buyer and sellers.

Received data: base case operating information, sink and source buses, TTC result from each area.

Sent data: quadratic expression of the PTDFS of tie-lines, system-wide TTC result.

2. Each Control Area

Each control area calculates its own P^{TTC} using repeated power flow method. The flowchart is shown in Fig. 2, which includes the following steps:
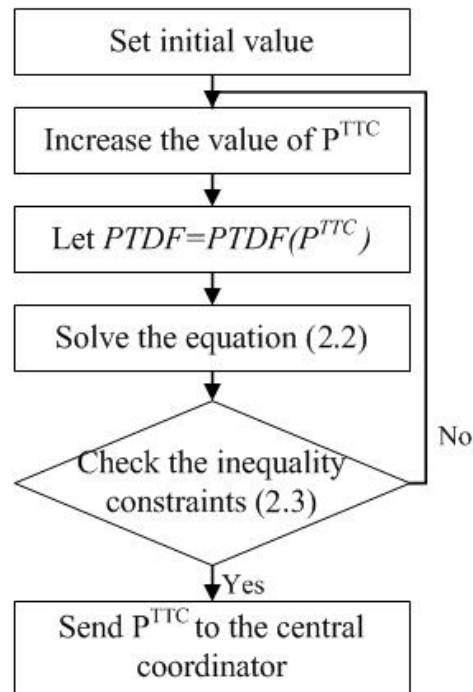
Fig. 2. Flowchart for each control area.

1. Set the repeated step of power flow analysis;

2. Increase the value of P^{TTC};

3. Update PTDFs and let $PTDFs = PTDFs(P^{TTC})$;

4. Solve the equality constraints (2.2);

5. Check whether any limits are violated, if yes, go to step 6; if not, go to step 2 and repeat the steps 2-5;

6. Stop and send the P^{TTC} of this area to the central coordinator.

   Received data: quadratic expression of the PTDFS of tie-lines.

   Sent data: local TTC computation result.
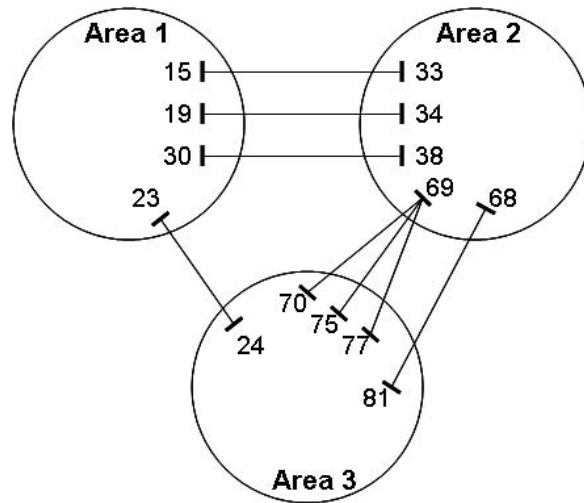
Fig. 3. IEEE 118-bus partitioned interconnected system.

Table I. Assumed line power flow limits of IEEE 118-bus system (RPF)

Line Code	Power Flow Limits (MW)
L7, L9, L13, L21, L31, L33, L38, L50, L90, L94, L96-99, L108, L110, L116, L123, L124, L137-139, L141, L142, L163, L183	800
L8, L32, L36, L51, L54, L93, L95, L102, L107, L127, L134	1000

E.   Numerical Results

The proposed two-level hierarchical computation scheme is validated on IEEE 118-bus test system. The system is divided into three areas each having about $35-40$ buses. The system partitioning and tie-lines are shown in Fig. 3. Voltage limits used are $0.90-1.10 p.u.$. The power flow limits used are 150 MW except for the lines listed in Table I. The incremental step is 1MW in repeated power flow.
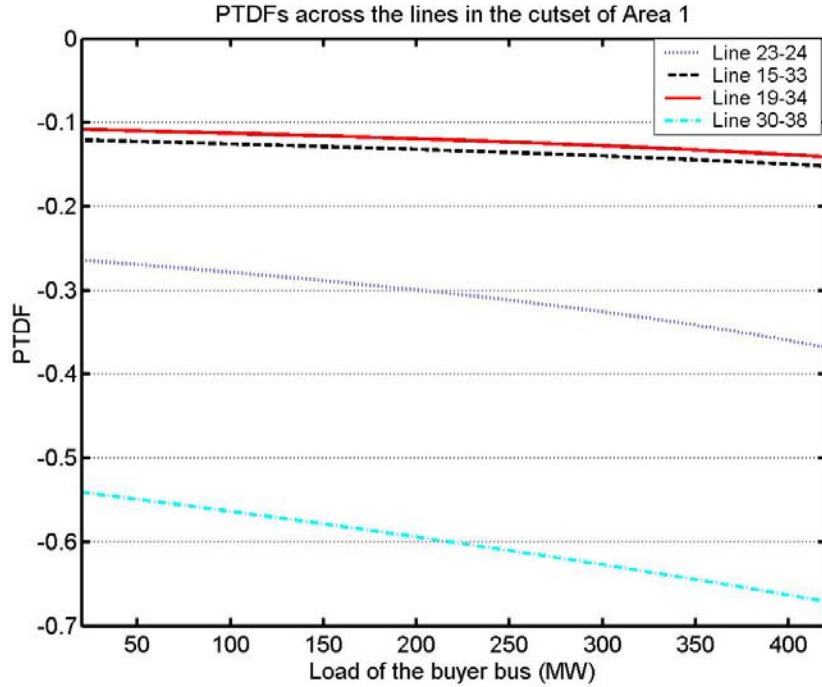
Fig. 4. PTDFs across the lines in the cutset of Area 1.

1. Single Transfer

Two cases are used to evaluate our approach. Case 1 is to find TTC between bus 69 (seller) in area 2 and bus 2 (buyer) in area 1. Case 2 is to find TTC between bus 69 (seller) in area 2 and bus 71 (buyer) in area 3.

Case 1:

The PTDFs changes are illustrated in Fig. 4. The figure shows typical distribution factors across the lines in the cut-set of Area 1 where the sink bus 2 is located. With the increase of the transfer from the source bus 69 to the sink bus 2, it is expected that these PTDFs experience considerable changes.

A comparison of results obtained with and without updating PTDFs are given in Table II. The limiting constraints are the voltage magnitude limit at bus 2 and the power flow limit on line 104, in areas 1 and 2 respectively. In area 3, the power

Table II. P_{Bus2}^{TTC} of different control areas

	Area1	Area2	Area3
P_{Bus2}^{TTC} (Updated)	443	320	644
P_{Bus2}^{TTC} (Not updated)	443	349	808
Limit Constraint	Bus 2	Line 104	Line 30

Table III. P_{Bus71}^{TTC} of different control areas

	Area1	Area2	Area3
P_{Bus71}^{TTC} (Updated)	974	958	748
P_{Bus71}^{TTC} (Not updated)	1210	1326	798
Limit Constraint	Bus 30	Line 119	Line 117

flow limit on the tie-line 30 which connects buses 23 and 24 is hit first.

Case 2:

The PTDFs changes are illustrated in Fig. 5. The figure shows typical distribution factors across the lines in the cut-set of Area 3 where the sink bus 71 is located. With the increase of the transfer from the source bus 69 to the sink bus 71, it is expected that these PTDFs experience considerable changes.

A comparison of results obtained with and without updating PTDFs are given in Table III. The limiting constraint in area 1 is the power flow limit on the tie-line 30 connecting buses 23 and 24; the limiting constraint in area 2 is the power flow limit on the tie-line 119 connecting bus 69 and bus 70; the limiting constraint in area 3 is power flow limit on line 117.

The results summarized in Table IV. It can be seen that if the PTDFs are updated as suggested in this chapter when calculating TTCs using multi-area two-level hierarchical algorithm, the results of the integrated and multi-area solutions will be
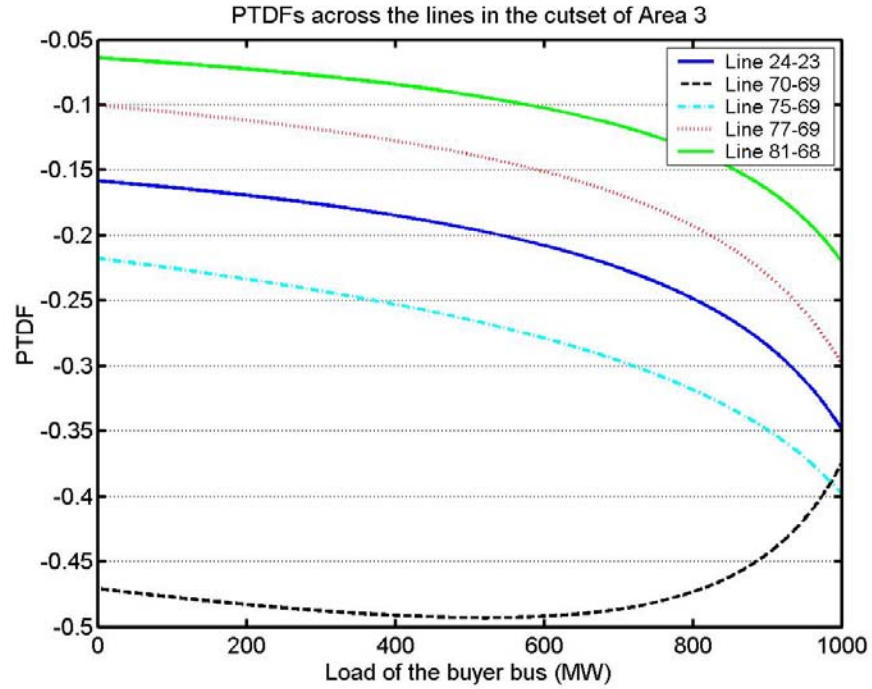
Fig. 5. PTDFs across the lines in the cutset of Area 3.

Table IV. Results of the integrated and multi-area calculation - single transfer

	Integrated System	Multi-area System (Updated)	Multi-area System (Not updated)
P_{Bus2}^{TTC}(MW)	320	320	349
Error		0.0%	9.0%
P_{Bus71}^{TTC}(MW)	729	748	798
Error		2.6%	9.5%

Table V. Simultaneous TTC of different control areas

	Area1	**Area2**	**Area3**
P_{Bus2}^{TTC}	443	279	568
P_{Bus71}^{TTC}	423	259	548
Limit Constraint	Bus 2	Line 104	Line 119

Table VI. PTDFs of single and simultaneous transfers to tie-lines

Tie-line	**Single Transfer case 1**	**Single Transfer case 2**	**Simultaneous Transfer**
15 to 23	-0.1208	-0.0216	-0.1424
19 to 34	-0.1081	-0.0239	-0.1321
30 to 38	-0.5407	-0.1072	-0.6478
23 to 24	-0.2642	-0.1584	-0.1058
69 to 70	0.1719	0.5005	0.6724
69 to 75	0.0978	0.2365	0.3344
69 to 77	0.1054	0.1039	0.2093
68 to 81	-0.0890	0.0638	-0.0252

very close, yielding an acceptable approximation. On the other hand, using constant PTDFs will yield errors which may be significant depending upon the operating point.

2.   Simultaneous Transfer

The simultaneous transfer case combines the above two single transfer cases. The seller bus is bus 69 in area 2 which is the slack bus in this case. The buyer buses are 2 (buyer) in area 1 and bus 71 (buyer) in area 3. Gradually increase load at bus 2 and 71 at 1 MW per step, respectively.

The results obtained with updating PTDFs are given in Table V. PTDFs of f t-lines on base case for single and simultaneous transfers are listed in Table VI. Compared with the single transfer cases, the TTC results are different. The reason

Table VII. Results of the integrated and multi-area calculation-simultaneous transfer

	Integrated System	Multi-area System
P_{Bus2}^{TTC}(MW)	279	279
P_{Bus71}^{TTC}(MW)	259	259

is that PTDF to a certain line are calculated by summing the PTDFs for all of the transfers to this line with the effect of simultaneous transfer.

The results summarized in in Table VII. It can be seen that the proposed PTDF-based decomposition method can also be extended to the simultaneous TTC studies.

F.   Conclusion

In this chapter, a quadratic approximation of nonlinear PTDFs which are derived by a Taylor series expansion is used to update PTDFs in TTC calculations of a multi-area system. The proposed updating method does not require numerical integration but just a single power flow solution. In the proposed hierarchical computation architecture, the PTDFs are updated to calculate nonlinear TTC in each area while a central entity coordinates these results to determine the final TTC value. This approach avoids information exchange between areas during the TTC calculation. Simulation results on the IEEE 118-bus system are used to validate the proposed method for both single and simultaneous TTC studies.

CHAPTER III

REI-EQUIVALENT BASED DECOMPOSITION ALGORITHM

A. Introduction

The transfer of power through a transmission network is accompanied by voltage drops between the generation and the loads. In some circumstances, in the seconds or minutes following a disturbance, voltages may experience large, progressive falls, which are so pronounced that the system integrity is endangered and power cannot be delivered correctly to customers. This situation is referred to as voltage instability and its calamitous result as voltage collapse.

In an increasing number of systems, voltage instability is recognized as major threat for system operation and planning, at least as important as thermal and voltage magnitude problems, considered in the Chapter II. At the other hand, contingency analysis aims at analyzing the system response to large disturbances that may lead to instability and collapse. While contingency analysis usually focuses on a particular operating point, it may be also desirable to determine how far a system can move away from this operating point and still remain in stable state.

A literature survey [27] on voltage instability problem concluded four methods to obtain loadability limits (transfer capability): Continuation Power Flow (CPF) [8–11,28], time simulation coupled with sensitivity analysis [29,30], VQ courves [31,32], and optimization methods [33–36]

In this chapter, we will use CPF method to calculate TTC with the consideration the contingencies, thermal limits, bus voltage limits, generator Q limits, and voltage stability limit. Generally, CPF execution is commonly undertaken by the Independent System Operator (ISO), which can access the entire network model and information.

In multi-area power system, a decentralized solution which is identical to the integrated system solution can be obtained by applying decomposition methods to a centralized problem. The decentralized method has been successfully used in DC power flow, RPF and OPF. In [20], a decomposition method based on linear Power Transfer Distribution Factors (PTDFs) is used to determine the multi-area TTC by decentralized DC load flow. This method is extended to nonlinear PTDFs and TTC is determined by decentralized RPF in [37]. Also, a distributed multi-area OPF method is described in [38]. Moreover, various decentralized OPF methods have been proposed for congestion management as reported in [39, 40]. However, the CPF has not been formulated in a decentralized framework yet.

There are two main contributions of this chapter. The first is a decomposition framework, where each area uses REI-type network equivalents to represent its neighbors. The second is a decentralized version of the CPF method to compute the TTC. In the proposed version, the continuation parameter is updated in a distributed but coordinated manner. The main objective of the proposed method is to allow each area to compute the entire system's TTC value without knowing the detailed operating data of other areas and thus to save the computation time.

B. Continuation Power Flow (CPF) for TTC Computation

CPF is a general method, which can yield a solution even at voltage stability points. Since this method is well documented in the literature [9, 10], it will be only briefly reviewed here.

The purpose of the continuation power flow was to find a continuum of power flow solutions for a given load change scenario. The general principle behind the continuation power flow is rather simple. It employs a predictor-corrector scheme to
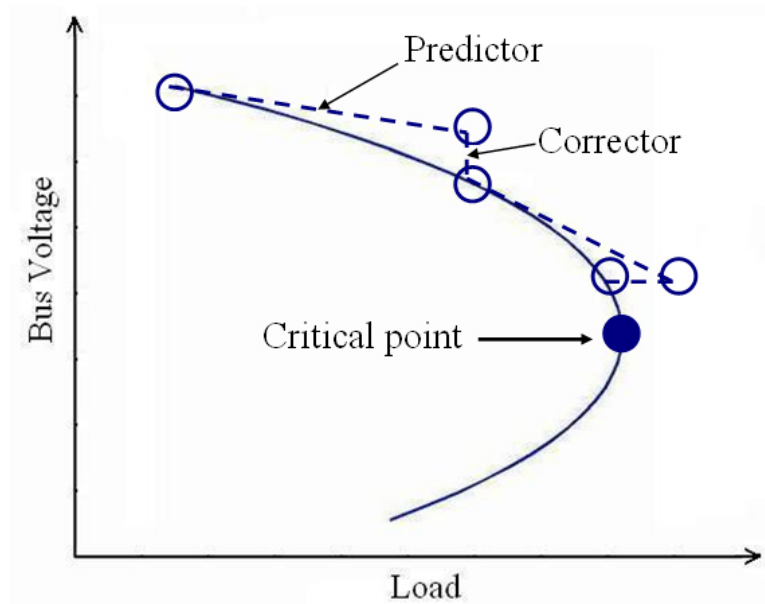
Fig. 6. An illustration of the predictorarrector scheme used in the continuation power flow.

find a solution path of a set of power flow equations that have been reformulated to include a load parameter. As shown in Fig. 6, it starts from a known solution and uses a tangent predictor to estimate a subsequent solution corresponding to a different value of the load parameter. This estimate is then corrected using the same Newton-Raphson technique employed by a conventional power flow. The local parametrization mentioned earlier provides a means of identifying each point along the solution path and plays an integral part in avoiding singularity in the Jacobian.

1. Review of the Locally Parametrization CPF

1) Reformulation of the Power Flow Equations: The net active and reactive injections at the sink and source buses are the function of λ

$$P_i = P_{i0} + \lambda K_{Pi} \tag{3.1}$$

$$Q_i = Q_{i0} + \lambda K_{Qi} \tag{3.2}$$

where λ is the parameter controlling the amount of injection; P_{i0}, Q_{i0} are the base case real and reactive power injections at bus i; K_{Pi}, K_{Qi} are the load participation factors, and the constant power load model will be considered.

The traditional power flow equations augmented by an extra equation for λ are expressed as:

$$f(\theta, V, \lambda) = 0 \tag{3.3}$$

where θ is the vector of bus voltage angles, and V is the vector of bus voltage magnitudes.

2) Predicting the Next Solution: The predictor with step length control provides an initial estimate of the state variables for the power flow solution for the next step increase in transfer power. Without a good starting approximation for each step, the power flow algorithm will fail to converge or converge to an extraneous solution. Once a base case (for λ=0) solution is found, the next solution can be predicted by taking an appropriately sized step in a direction tangent to the solution path. The tangent vector $t = [d\theta \ dV \ d\lambda]^T$ is derived

$$d[f(\theta, V, \lambda)] = f_\theta d\theta + f_V dV + f_\lambda d\lambda \tag{3.4}$$

Since (4.4)is rank deficient, an arbitrary value such as 1 can be assigned as one of the elements of the tangent vector $t = [d\theta \ dV \ d\lambda]^T$, i.e., $t_k = \pm 1$. Then

$$\begin{bmatrix} f_\theta & f_V & f_\lambda \\ & e_k & \end{bmatrix} [t] = \begin{bmatrix} 0 \\ \pm 1 \end{bmatrix} \tag{3.5}$$

where e_k is a row vector with all elements zero, except for the kth entry that is equal

to 1.

The prediction will then be computed as

$$
\begin{bmatrix} \theta^* \\ V^* \\ \lambda^* \end{bmatrix} = \begin{bmatrix} \theta \\ V \\ \lambda \end{bmatrix} + \sigma \begin{bmatrix} d\theta \\ dV \\ d\lambda \end{bmatrix} \tag{3.6}
$$

where $*$ denotes the predicted solution for the next value and σ is a scalar used to adjust the step size.

2. Choosing the Continuation Parameter

The largest element of the tangent vector is assigned as the continuation parameter

$$
x_k : |t_k| = max\{|t_1|, |t_2|, \ldots, |t_m|\} \tag{3.7}
$$

where t is the tangent vector with a corresponding dimension $m = 2n_1 + n_2 + 1$, where n_1 and n_2 are the number of P-Q and P-V buses, respectively. The index k corresponds to the maximum component of the tangent vector.

3. Parametrization and the Corrector

The corrector is a slightly modified Newton power flow algorithm in which the Jacobian matrix is augmented by an equation to account for the continuation parameter. Because the number of state variables for power flow solution is unchanged, it is necessary, at each step of CPF, to select and assign a value to one variable of x. This is called local parameterizations. The selection and assigned value are made by CPF.

Let $x = [\theta \ V \ \lambda]^T$ and $x_k = \eta$; then, the new set of equations will take the form

$$
\begin{bmatrix} f(x) \\ x_k - \eta \end{bmatrix} = [0] \tag{3.8}
$$

where η is an appropriate value for the kth element of x. A modified Newton power flow is used to solve (4.22).

C. Integrated System TTC computation

A practical CPF implementation considers contingencies and the effects of physical and operating limits in the integrated system TTC calculation. The calculator obtains the current system state from the State Estimator (SE). A contingency list is obtained from the Security Analysis (SA) function. Load forecasters, generation schedules and outage equipment information are provided by the Current Operating Plan (COP). The result is posted at the Open Access Same-Time Information System (OASIS). The following is a summary of the steps for determining the TTC for a specific source/sink transfer case.

1. Input power system data.

2. Select the contingency from the contingency list.

3. Initialize:

   (a) Run power flows to ensure that the initial point does not violate any limits.

   (b) Set the tolerance for the change of transfer power.

4. Prediction step of CPF:

   (a) Correction the tangent vector $t = [d\theta \ dV \ d\lambda]^T$.

    (b) Choose the scalar σ to design the prediction step size.

    (c) Make a step of increase of the transfer power to predict the next solution using equation (4.6).

5. Correction step of CPF with generator Q limits. Solve the equation (4.22).

6. Check for limit violations:

   Check the solution of the step 5 for violations of operational or physical limits– line flow limit, voltage magnitude limit, and voltage stability limit. If there are violations, reduce the transfer power increment by $\sigma = 0.5\sigma$, then go back to step 5 until the change of the transfer power is smaller than the tolerance. The maximum transfer power for the selected contingency is reached. Otherwise, go to the prediction step 4.

7. Check if all contingencies are processed. If yes, compare the maximum transfer powers for all the contingencies and choose the smallest one as the TTC for this specific source/sink transfer case and terminate the procedure. Otherwise, go to step 2.

D. Decomposition of the System

The main challenge in decomposing a multi-area system into areas is to find proper coupling constraints between areas. In this paper, a new decomposition scheme based on the REI-type equivalents is developed.

1. System Decomposition

In a multi-area system, it is assumed that each area operates autonomously by its own independent operator. Each area carries out its own CPF calculation and main-
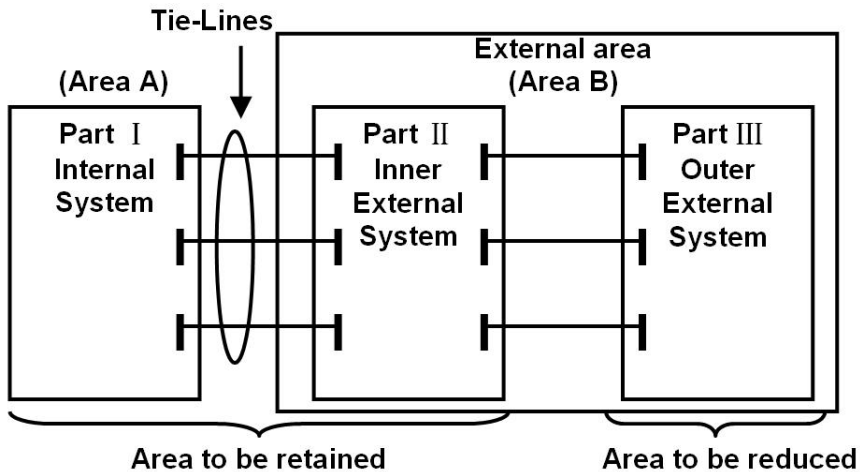
Fig. 7. Interconnected system divided into three parts.

tains its own detailed system model. Furthermore, each area uses network equivalents to represent the buses in other areas except for the boundary buses, the seller bus and the buyer bus whose identities are maintained by excluding them from the equivalents.

Two-area-interconnected system is illustrated as an example to introduce the decomposition method detailed in Fig. 7. The system can be divided into three parts: 1) internal area; 2) inner external area which includes boundary buses incident to internal area; and 3) outer external area. Considering area A operation, parts 1) and 2) will be modeled in detail and part 3) will be reduced to an equivalent network. The sending and receiving buses of this system should be retained, since the load and generation at these buses will have to be modified when solving the CPF.

2. Review of the REI-Type Equivalents

Among various equivalent techniques that appeared in the literature [41], REI-type equivalents are chosen here for two reasons: 1) the bus identities (types) are not lost but represented in an aggregated form when replaced by the REI-nodes, and 2) the reactive power can be provided by the equivalents more accurately especially

around the base case operation. Therefore, more accurately results can be obtained when considering the voltage problem.

REI-type equivalents are developed by Dimo [42], and later introduced to the U.S by Tinney and Powell in [43]. The basic idea of the REI equivalent is to aggregate the injections of a group of buses into a single bus. The aggregated injection is distributed to these buses via a radial network called the REI network. After the aggregation, all buses with zero injections are eliminated yielding the equivalent. The procedure of obtaining an REI equivalent consists of two steps:

1. As shown in Fig. 8, construct and REI network from the base case power flow solution and attach it to the buses to be eliminated. The admittance values, Y_i, net complex power injection at the R bus, S_R and its voltage V_R are given as:

$$Y_i = \frac{-S_i^*}{|V_i|^2}, \ i = 1, \ldots, n \tag{3.9}$$

$$S_R = \sum_{i=1}^{n} S_i \tag{3.10}$$

$$V_R = \frac{S_R}{\sum_{i=1}^{n} (S_i/V_i)}; \quad V_G = 0 \tag{3.11}$$

$$Y_R = \frac{S_R^*}{|V_R|^2} \tag{3.12}$$

where S_i is the net complex power injected at bus i.

2. Eliminate the bus 1,2,...,n and bus G by Kron reduction and obtain the equivalent network model.

It is often desirable to construct more than one REI network for the external system. [44] suggested that loads should be aggregated to an REI network and gen-
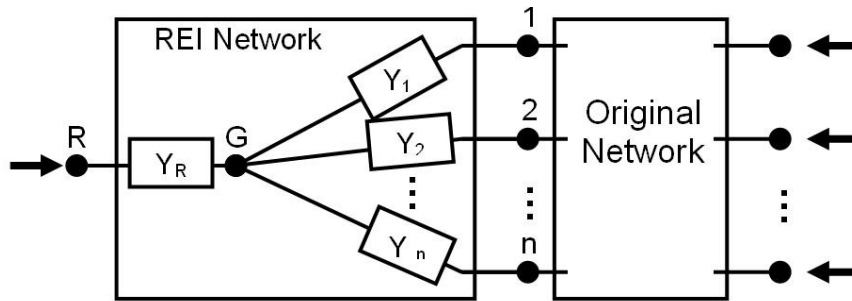
Fig. 8. REI network attached to the original network.

erations should be aggregated to a different REI network for accuracy. Since the eliminated passive nodes will be represented by a single REI node, these nodes are grouped based on their type (PQ or PV). In this study, all PV and PQ buses except for the seller and buyer buses of outer external area are grouped into two different REI equivalent networks which are assigned the corresponding bus types (PQ or PV) accordingly.

E.   Multi-Area TTC Computation

Using the above decomposition method, operators in all areas can compute system-wide TTC without exchanging the information between each other. However, the admittances of the REI network are functions of the operating point for which the equivalent is constructed. Doing so will also introduce errors in the multi-area TTC result. In light of this, the equivalent has to be properly updated during the TTC computation. In [45], Dy Liacco, Savulescu and Ramarao proposed an X-REI equivalent with a calibrating network which is used for the boundary mismatching. In [46], Dopazo, Irisarri and Sasson proposed an S-REI equivalent where the REI-node voltage and the equivalent network parameters are updated.

A different method to update the REI network is proposed here. The criteria

for updating REI network are the maximum mismatch of the tie line power flows and buyer bus voltages from different areas. In order to implement that method, which requires comparison of the tie line power flows and buyer bus voltage, the computations of each area must be synchronized.

In the case of the decentralized RPF implementation, the increment of transfer power is fixed. It is easy for different area to achieve synchronism. Each area calculates its own TTC using the equivalent system by using the repeated incremental power flow approach. If an update flag is received from the central coordinator, each control area will update and rebuilt its equivalent by means of current operating point and send it back so that they are re-broadcasted to all other areas. The central coordinator simply runs a single power flow for the base case. During the multi-area TTC computation, the central coordinator only monitors the tie-line power flows and receiving bus voltage magnitude. It does not know or need the detailed operating information of each area.

In the case of the decentralized CPF implementation, each area carries out its own CPF and the continuation parameter for each area may be different at each step. Therefore, a strategy for choosing and updating the continuation parameter which ensures synchronized CPF calculation in different areas is introduced.

1. Choice and Updating of the Continuation Parameter

A self-adaptive step size control is implemented for the sink area. Λ is chosen as the continuation parameter when starting from the base case. Then the continuation parameter is chosen from the voltage increment vector. A constant voltage magnitude decrease is used to predict the next solution. Usually, the scalar σ in (4.22) is set as 0.02. Therefore, a constant decrease in voltage magnitude will result in a large increase in load at the beginning and a small increase in load as the nose point is

approached.

After each correction step, the load change at the sink area will be broadcast to all other areas. The continuation parameter remains to be λ in all other areas, and the scalar σ is set as the load change of the sink area at each step. Hence, different areas will have the same load increase at each discrete step of CPF calculation.

For the areas where the prediction step is not parameterized, voltage stability violation is decided based on whether or not the correction steps converge. If the prediction step is too large and the correction step does not converge, it will imply the violation of voltage stability limit in this area. In such a case, this area will broadcast the limit violation signal to all other areas. The power transfer increment will be reduced by half before the process resumes.

2.   Generator Reactive Power Limits

Another issue related to updating the equivalents is the generator reactive power limits. As the power transfer increases at a chosen PQ bus, generator buses will continue to hit their Q limits in succession. As each limit is reached, the generated reactive power will be held at the Q limit, bus type will be switched to PQ and.the bus voltage will become an unknown increasing the dimension of the Jacobian by one. While updating the equivalents, these generator buses which are now of type PQ are grouped with other PQ buses in each area. This will continue until other limits are reached.

3.   Contingencies Issue in Multi-Area System

Contingencies associated with the tie-lines must be co-monitored by all areas. However, contingencies caused by topology changes within individual areas do not have to be modeled directly by others. Instead, when a contingency occurs within one

area, only the network model of this area will be changed first by its area computer. Since, the other areas will not be informed about this contingency, they will not take any action. As a result, the tie-line power flows and buyer bus voltages calculated from different areas will have very large mismatches during the synchronized computation. After updating the equivalents for the area experiencing the contingency, the updated equivalent buses will reflect the effects of the contingency. This way, other areas can account for the effects of the contingency indirectly.

The contingency analysis will be carried out in a pre-specified sequence. First, the contingencies occurring in tie-lines will be analyzed and co-monitored by all areas. Then, the other contingencies occurring within individual areas will be analyzed that area at a time.

4. Proposal Procedure

The proposed method assumes that areas do not share their network data such as current system state, contingencies, and operating or physical limits; however they are willing to cooperate via a central coordinator for system wide computations such as TTC.

Procedure followed by the central coordinator: The central coordinator does not know or need the detailed operating information of each area. The flowchart is shown in Fig. 9. The central coordinator executes five functions:

(a) Run the base case power flow, and read the power flow data and the transfer case to build the computation model for each area by REI equivalents.

(b) Build the contingency list of tie-lines and distribute it to each area.

(c) Compare the tie line and receiving bus information from each area and send the update flags to each area.

(d) Distribute the load change of each step at the sink area to other areas.
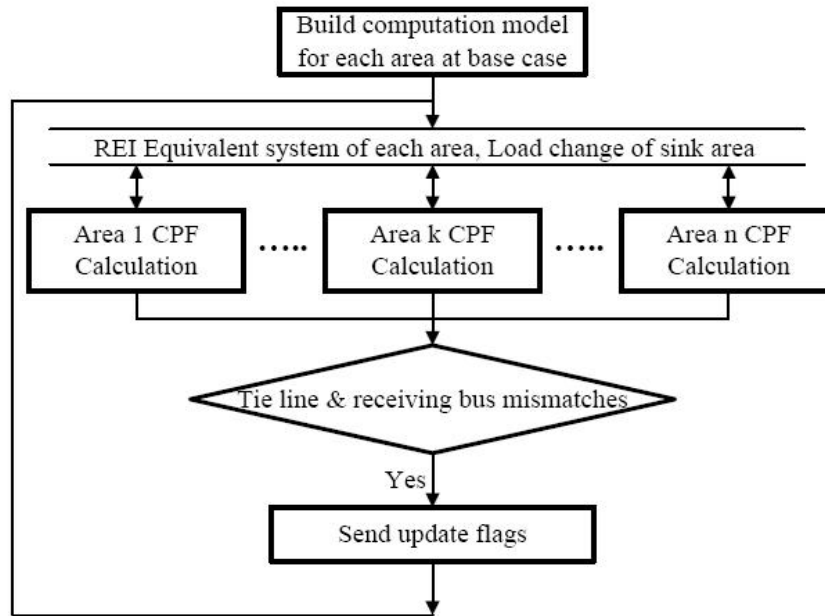
Fig. 9. Flowchart for central coordinator.

(e) Distribute the equivalents if there are update flags.

Received data: Load change of sink area at each step, all tie line real power flows, receiving bus voltage, and updated area equivalents if update flag is up.

Sent data: Contingency list of tie-lines, base case computation model for each area, tolerance for the change of transfer power, load change of sink area at each step, update flag, and updated area equivalents if update flag is up.

Procedure to be carried out by each area: Each area carries out its CPF calculation by using the equivalent system of other areas. Computations at each area must be synchronized. The detailed computation steps of each area block for determining TTC are:

(a) Input data. Receive the computational model at base case, the contingency list of tie-lines, and the tolerance for the change of transfer power from the central coordinator.

(b) Select a contingency following the sequence described in section E.2.

(c) Check the update flag. If there is no update flag from the central coordinator, go to step (e); else, continue.

(d) Update the computation model and then continue.

    (i) Build an REI equivalent for its own system.

    (ii) Send the equivalent to the coordinator, which in turn distributes it to all other areas.

    (iii) Receive the equivalents of all other areas.

    (iv) Build its computation model.

(e) Prediction step of CPF. If it is the sink area, the continuation parameter is chosen from the voltage increment vector . Choose the scalar to design the prediction step size. If it is not the sink area, the continuation parameter is always the power increment vector . This step increase of the transfer power will be decided by the sink area's load change.

(f) Correction step of CPF with generator Q limits. If it is the sink area, the load change should be sent to the central coordinator after the correction step.

(g) Check for limit violations. If there are violations, broadcast the limit violation signal to other areas and all areas reduce the transfer power increment by half and go back to correction step (f). If the change of the transfer power is smaller than the tolerance, this is the maximum transfer power for the selected contingency. Otherwise, go to next step.

(h) Send the tie line real power flows and buyer bus voltage to the coordinator. Then go to step (c).

(i) Is this the last contingency? If yes, compare the maximum transfer powers for the selected contingencies and choose the smallest one as the TTC for the specific source/sink transfer case. Otherwise, go to step (b).

Table VIII. Assumed line power flow limits of IEEE 118-bus system (CPF)

Line Code	Power Flow Limits (MW)
L8-9, L9-10, L2-12, L15-17, L16-17, L23-25, L25-27, L8-30, L26-30, L23-32, L34-37, L60-61, L63-64, L38-65, L64-65, L49-66, L49-66, L69-70, L70-71, L69-75, L77-80, L88-89, L89-90, L89-92, L100-103, L68-116	800
L5-8, L25-26, L17-30, L37-38, L59-63, L61-64, L65-66, L68-69, L80-81, L86-87	1000

Received data: contingency list of tie-lines, base case computation model, tolerance for the change of transfer power, load change of the sink area, update flag, and other area REI equivalents if update flag is up.

Sent data: load change of sink area, tie line real power flows, receiving bus voltage magnitude, and area's updated REI equivalent if update flag is up.

F.   Numerical Results

The proposed method is tested on IEEE 118-bus test system. The system is divided into three control areas as Fig. 3. One hundred seventy-seven contingencies are analyzed in the following sequence: first, eight contingencies occurred in tie-lines; second, 45 contingencies within area 1; third, 61 contingencies within area 2; fourth, 63 contingencies within area 3. Line flow, voltage magnitude, generator Q and voltage stability limits are considered for this multi-area TTC computation. The generator Q limits are given in the test case. The voltage limits used are $0.85 - 1.10$ p.u. The power flow limits used are 150 MW except for the lines listed in Table VIII. Two cases are given in detail for illustrating contingency occurred in tie-line and the contingency occurred within area 1.
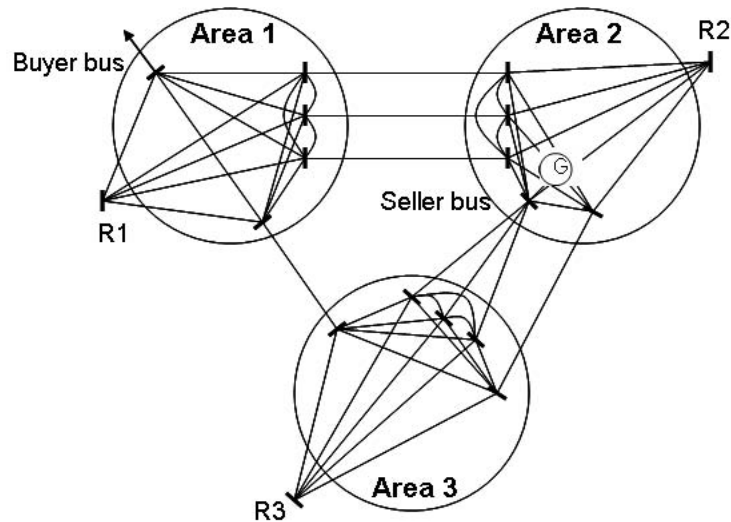
Fig. 10. Situation after REI-equivalent-based decomposition.

The transaction between seller bus 69 in area 2 and the buyer bus 16 in area 1 is illustrated here. Based on the base case integrated system power flow result, each area builds its own REI equivalent system. In each area, there equivalent branches connecting boundary buses, REI nodes, and receiving/sending buses. The system decomposition result based on REI-type equivalent is shown in Fig. 10. $R1$, $R2$, and $R3$ refer to the REI equivalent buses. Each one includes one PV equivalent bus and one PQ equivalent bus. Then, the equivalent model is distributed to other areas. Each area makes use of its detailed model and REI-type network equivalents of the other areas in building its computation model and then carries out the CPF calculation. The tolerance for the change of the transfer power is set as 0.01 MW. The scalar σ is set as 0.02 for for the sink area. The error limit is set as 4%. Therefore, 6 MW (4% of the line power flow limit) is chosen as the tie line mismatch limit and 0.04 p.u. as the receiving bus voltage magnitude mismatch limit to be used for deciding whether or not to update area equivalents.

Tie-line Outage Contingency: The first illustrated contingency is the outage of

Table IX. Generator buses at maximum reactive power output

Load of buyer bus (MW)	Area1	Area2	Area3
25.00	19,32	34	92,103,105
37.35	12,19,32	34	92,103,105
155.60	12,19,32		92,103,105
187.28	12,15,19,32		92,103,105

tie-line $23-24$ which connects area 1 and area 3. This contingency is ranked the highest among all 8 contingencies that involve tie-line outages for the chosen power transfer case. The contingency should be analyzed and co-monitored by all three areas. Each area uses the computation model from the base case and selects this contingency. Table IX shows the generators reaching their Q limits at different load levels. For example, at the initial point, generator buses 19 and 32 in area 1 reach their Q limits. These buses are grouped with other PQ buses in area 1 into bus 120, which is a PQ equivalent bus representing all PQ buses in area 1.

Areas carry out their multi-area TTC computations. When the load of buyer bus reaches 120.97 MW, the buyer bus voltages calculated by area 1, area 2 and area 3 are 0.9389, 0.9050 and 0.8983 respectively. Therefore, the bus voltage mismatch limit is violated and REI equivalents of areas need to be updated. At this load level, generator bus 12 in area 1 reaches its Q limit and it will be grouped into bus 120. When the load of the buyer bus reaches 187.28 MW, REI equivalents of areas are updated again. Generator bus 15 in area 1 which reaches its Q limit will be grouped into bus 120. The updating scheme of area 1 is shown in Fig. 11. The solid line marked by squares is the PV curve of bus 122, a PQ equivalent bus which represents the PQ buses in area 2. Its voltage is updated from point A (0.9820) to B (0.9997), and from C (0.9885) to D (1.0024).

The updating scheme of area 2 is shown in Fig. 12. The solid line with square
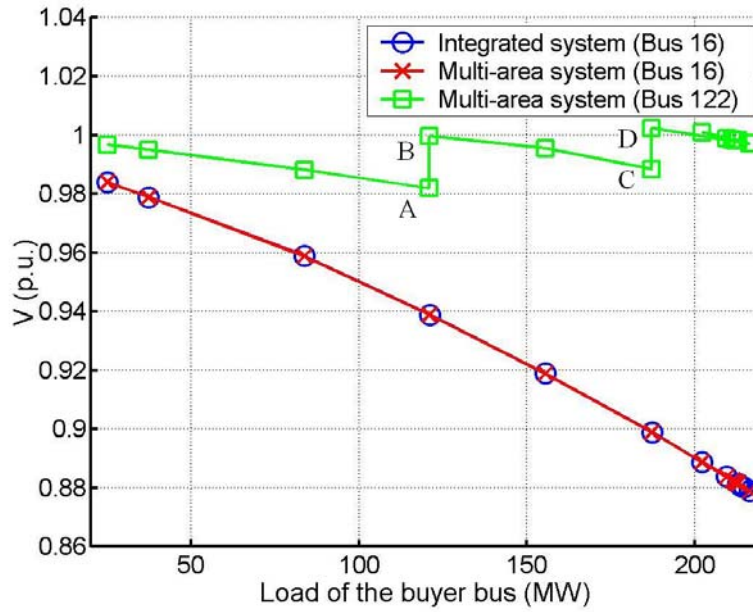
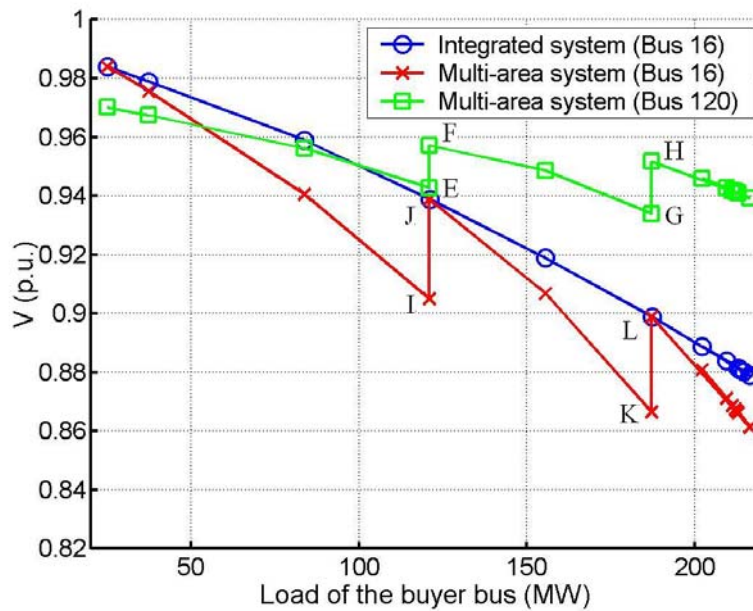Fig. 11. Comparison of PV curves calculated by area 1 and integrated system.

Fig. 12. Comparison of PV curves calculated by area 2 and integrated system.

mark is the PV curve of bus 120. Its voltage is updated from E (0.9427) to F (0.9572), and from G (0.9340) to H (0.9517). The voltage of the buyer bus, the solid line with cross mark, is updated from I (0.9050) to J (0.9389), and from K (0.8665) to L (0.8989). This mismatch will not lead to wrong voltage limit violations because area 2 only checks voltage limits for the buses within area 2 while bus 16 belongs to area 1.

When the load of buyer bus reaches 212.78 MW, the power flow limit of the line from bus 65 to bus 68 is hit in area 2. Therefore, the maximum transfer power calculated by our proposed method is 212.78 MW for this selected contingency. In the integrated system, the value is 213.26 MW with the same limit. The power flow solution comparison between the multi-area system and the integrated system is illustrated in Fig. 11. The solid line with cross mark and the solid line with circle mark are the PV curves of bus 16 computed by our proposed method and integrated method, respectively.

Next illustrated contingency is the outage of line 12-16 in area 1. This contingency is ranked highest among the rest of 169 contingencies for this specific transfer case. At the beginning, each area uses the base case model to calculate the TTC. Then, area 1 introduces this contingency while other areas remain unaware of the details of this contingency. Then, three areas continue their TTC computations. Table X shows the voltage magnitude of equivalent bus 120 before and after updating. Bus 120 is a PQ equivalent bus which represents the PQ buses in area 1, and reflects the effects of the contingency. As the load of the buyer bus is increased, generator buses 19, 32, 34, 92, 103, and 105 always hit their Q limits.

The maximum transfer power calculated by our proposed method is 91.71 MW for which the voltage magnitude of bus 16 is the binding limit. In the integrated system, this value is found as 90.85 MW with the same binding limit.

Table X. Voltage magnitude of equivalent bus 120

Step	Load of buyer bus (MW)	Voltage magnitude before update (p.u.)	Voltage magnitude after update (p.u.)
1	65.32	0.9611	0.9694
2	75.85	0.9617	0.9693
3	85.42	0.9605	0.9692
4	94.22	0.9599	0.9691

Table XI. Comparison of TTC value of CPU time for these two methods

Path	Method	TTC (MW)	CPU time (minutes)
69→16	Integrated	90.85	4.12
	Multi-area	91.71	2.92
69→2	Integrated	87.71	3.81
	Multi-area	88.28	2.71
69→28	Integrated	102.20	3.92
	Multi-area	104.34	2.45
69→86	Integrated	63.23	4.07
	Multi-area	64.76	2.87
69→106	Integrated	78.09	3.85
	Multi-area	78.92	2.67

Table XI shows the comparison of TTC value and CPU time for three different power transactions. All calculations are conducted on a Pentium IV 2.4-GHz personal computer using a program developed in MatLab. The multi-area TTC computation is assumed to be implemented in such a way that areas carry out their computations simultaneously. The communication time between areas and central coordinator is assumed negligible. Based on these assumptions, the simulation results appear in favor of the multi-area solution scheme.

G. Conclusion

A method for calculating the TTC in a large interconnected multi-area power system is presented. The method assumes that areas do not share their network data among themselves; however they are willing to cooperate via a central coordinator for system wide computations such as TTC. The proposed method evaluates TTC by taking into account contingencies and the effects of power system physical and operating limits on the line flows and voltage magnitude, generator reactive power, as well as the voltage stability limit. It uses the CPF as the computational tool and presents an implementation scheme where the computations are carried out in a distributed manner among the individual area computers. This is accomplished by the use of REI equivalents with a novel updating scheme, which is accomplished with limited data exchange between areas. Simulation results on the IEEE 118-bus system using integrated and proposed multi-area methods are provided for validation.

CHAPTER IV

A DECOMPOSITION ALGORITHM FOR MULTI-AREA OPF PROBLEM

A. Introduction

Optimal Power Flow (OPF) problem has been extensively studied and algorithmic improvements have been developed since its introduction in the early 1960's [12,13]. Hence, OPF solution techniques are quite mature and are widely used in minimizing generation cost and/or overall system losses [13]. Furthermore, these methods play a crucial role in the current deregulated environment due to their potential to optimally distribute the resources and thus yielding significant economic benefits to both power suppliers and customers. OPF problem formulation can account for the system constraints including AC load flow equations, transmission line thermal limits and voltage limits. Other considerations concerning pricing can also be incorporated into the formulation as well [47]. Several algorithms have been proposed to solve the OPF problem [13, 48].

OPF solution methods proposed so far are based on the assumption that the calculations will be commonly undertaken by the Independent System Operator (ISO), which can access the entire network model and its current economic information. On the other hand, it is recognized that a decentralized solution which is identical to the integrated system solution can be obtained by applying decomposition methods to a centralized problem.

Recently, a decomposition method is successfully used to solve the DC power flow and OPF problems where there are limited data and information exchange between different areas. In [20], a decomposition method based on linear Power Transfer Distribution Factors (PTDFs) is used to determine the multi-area total transfer ca-

pability (TTC) by decentralized DC load flow solution. Areas do not share their operating information yet the integrated system TTC can be calculated. Biskas [40] and Wang [39] approach the decomposition problem by dividing the system into regional sub-problems through tie-line price exchange or dummy buses. The integrated system's maximum social benefit can be calculated by limited information exchange. These techniques [20, 39, 40] decompose the network model according to each area's geographical boundaries. In other words, the tie-lines between areas are split and artificial variables are used to match the flows on both sides of tie lines. Inter-area exchange contracts within a market are difficult to manage using this approach and the disconnected network model.

The EPRI proposal [49] suggests that a common power system model is necessary and the decision variables of each Regional Transmission Organization (RTO)'s control area have to be solved iteratively. The proposed coordination method also calls for extensive data sharing among the RTOs such as the reduced equivalent of areas, the bid data, etc.

An application of Lagrangian relaxation to solve a multi-area decentralized DC nonlinear OPF is described in [50, 51]. Another alternative is presented in [38, 52] where a Lagrangian relaxation method based on "auxiliary problem principle" is used to parallelize the OPF problem solution. All these methods assume that there are one or more fictitious buses per tie-line. Then the coupling constraints are added into the objective function. A mechanism is required to update the Lagrange multipliers so that the dual problem can be optimized.

In this chapter, the traditional OPF is treated as the optimization problems with global variables. A new decomposition algorithm [53] based on the use of quadratic penalty functions is applied to solve this kind of problems. In addition, the solution is proposed to be implemented using a two-level computational architecture.

B.   General OPF Problem

In this work, it is assumed that the OPF problem is "smooth" with no discrete variables or controls. The objective function is the total cost of read and/or reactive generation. These costs may be defined as polynomials or as piecewise-linear functions of generator output. The problem is formulated as follows. The notion used in the model is:

ν the vector of voltage magnitude of buses,

θ the vector of voltage phase of buses,

S_{ij} the apparent power flow through line ij,

V_i the voltage magnitude in bus i,

S_{ij}^{max} the maximum transmission capacity of line ij,

P_{gi}, Q_{gi} the active and reactive power produced by generator i,

P_{Li}, Q_{Li} the active and reactive power demand in bus i,

V_i^{max}, V_i^{min} the maximum and minimum voltage magnitude in bus i,

$P_{gi}^{max}, P_{gi}^{min}$ the maximum and minimum active power production capacity of generator i,

$Q_{gi}^{max}, Q_{gi}^{min}$ the maximum and minimum reactive power production capacity of generator i.

$$\min_{P_g, Q_g} \sum f_{1i}(P_{gi}) + f_{2i}(Q_{gi}) \tag{4.1}$$

$$s.t. \quad P(v, \theta) - P_{gi} + P_{Li} = 0 \tag{4.2}$$

$$Q(v, \theta) - Q_{gi} + Q_{Li} = 0 \tag{4.3}$$

$$|\tilde{S}_{ij}| \leq S_{ij}^{max} \tag{4.4}$$

$$V_i^{min} \leq V_i \leq V_i^{max} \tag{4.5}$$

$$P_{gi}^{min} \leq P_{gi} \leq P_{gi}^{max} \tag{4.6}$$

$$Q_{gi}^{min} \leq Q_{gi} \leq Q_{gi}^{max} \tag{4.7}$$

where f_{1i} and f_{2i} are the costs of active and reactive power generation respectively, for generator i at a given dispatch point. Both f_{1i} and f_{1i} are assumed to be polynomials or piecewise-linear functions. (4.2) and (4.3) are the active and reactive power balance equations. (4.4) is the apparent power flow limit of lines. (4.5) is the bus voltage limits. (4.6) and (4.7) are the active and reactive generation limits.

C. Non-convex Property

The issue of convexity for the OPF problem has been discussed some in the literature [54–56]. In section, I use an example in [56] to discuss the non-convex property of the general OPF problem with voltage constraints. Convexity is a mathematical property of a set that states that if one constructs a line between any two points in the set, all the points on the line will also belong to the set. The word *convexity* also describes a property of certain function. A function $g(x)$ is said to be convex if for all x_1 and x_2 contained in a convex set, $g((1 - \mu)x_1 + \mu x_2) \leq (1 - \mu)g(x_1) + \mu g(x_2)$. These important properties have been exploited in different ways to establish other properties (such as "revenue adequacy" mentioned above) and to develop efficient optimization routines.

Consider an optimization problem cat in the following way:

$$\min_{P} C(P) \tag{4.8}$$

subject to

$$f(P) \leq 0 \tag{4.9}$$

where P is a vector of variables, $C(P)$ is a scalar cost function expressed in terms

of P, and $f(P)$ is a vector of constraints imposed on P that limits the values P may take. If $C(P)$ is a convex function and the feasible set $\Omega = P : f(P) \le 0$ is also convex, then efficient algorithm exist to find an optimal solution, and the solution is guaranteed to be either unique or to belong to a continuous set of adjacent (feasible) minimal cost solution. If either the cost function or the feasible set is not convex, then practical algorithms are not generally available to find the globally optimal solution. Only locally optimal solutions can be guaranteed. (It is shown in [57] that misapplication of sophisticated algorithm such as lagrangian relaxation can result in suboptimal or infeasible answers, when the problem should exhibit a unique globally optimal answer.)

If practice, it is implicitly defined by the more general constraints

$$f(P, Q, V) \le 0 \tag{4.10}$$

where P, Q and V, respectively active power, reactive power, and voltage phasor. The voltage phasor may be represented in polar or rectangular coordinates. Given the nonlinear form of equality and inequality constraints contained in (4.10), it should not be expected that this optimization problem should be convex. Since many typical and practical optimization problems focus only on active power, we can theoretically examine the projection of the set described by (4.10) onto active powers P to obtain (4.9). This resulting feasible set is a best-case representation since it may appear convex while the underlying representation with more variables may not be. If the feasible set described by (4.10) is not convex, then optimization algorithms may exhibit computational problem, as mentioned earlier. Nevertheless, if the projected feasible set described by (4.9) is convex, regardless (4.10), one can establish useful theoretical properties.

Let us turn to the power flow equations. These are constructed directly from the
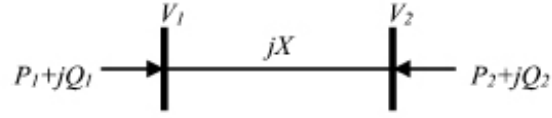
Fig. 13. Two-bus system.

current injection equations by multiplying currents and voltage s to obtain power

$$
\begin{bmatrix} P_1 + jQ_1 \\ \vdots \\ P_N + jQ_N \end{bmatrix} = \begin{bmatrix} V_1 & & \\ & \ddots & \\ & & V_N \end{bmatrix} \begin{bmatrix} Y_{11}^* & \cdots & Y_{1N}^* \\ \vdots & \ddots & \vdots \\ Y_{N1}^* & \cdots & Y_{NN}^* \end{bmatrix} \times \begin{bmatrix} V_1^* \\ \vdots \\ V_N^* \end{bmatrix} \tag{4.11}
$$

or for each bus

$$
P_i + jQ_i = V_i \sum_{k=1}^{N} Y_{ik}^* V_k^* \tag{4.12}
$$

To demonstrate that the set of power injections that satisfy (4.11) is not convex when minimum and maximum voltage constraints are imposed, we consider an elementary two-bus system and show that the set of feasible injections is not convex. We argue that this is sufficient to demonstrate problems with convexity for general power system, because we can choose feasible operating conditions on a general system that allow it to be reduced to an equivalent two-bus system.

To this end, consider the two bus system shown in Fig. 13. The two buses are connected through a lossless transmission line with reactance X. We neglect losses, but the reader will observe that the fundamental results that follow do not change with the addition of losses. The relevant power flow equations for this system are

$$
P_1 + jQ_1 = \frac{jV_1}{X}(V_1^* - V_2^*) \tag{4.13}
$$

$$
P_2 + jQ_2 = \frac{jV_2}{X}(V_2^* - V_1^*) \tag{4.14}
$$

Now we need to specify two specific feasible solutions to consider. Analogous to the current injection example of the previous section in which we reversed the current flow, here we choose feasible operating points that reverse the active power flow while keeping the reactive power constant. Let us define V_m to be the greater of the two minimum voltage limits for the two buses. The two cases we propose here are as follows.

Feasible Point A: $V_1 = V_m e^j 0 = V_m$ and $V_2 = V_m e^j \pi/2 = jV_m$, **giving**

$P_{A1} = -\frac{V_m^2}{X}$, $Q_{A1} = \frac{V_m^2}{X}$

$P_{A2} = \frac{V_m^2}{X}$, $Q_{A2} = \frac{V_m^2}{X}$

Feasible Point B: $V_1 = V_m e^j 0 = V_m$ and $V_2 = V_m e^j 3\pi/2 = -jV_m$, **giving**

$P_{B1} = \frac{V_m^2}{X}$, $Q_{B1} = \frac{V_m^2}{X}$

$P_{B2} = -\frac{V_m^2}{X}$, $Q_{B2} = \frac{V_m^2}{X}$

From (4.13) and (4.14), candidate injections at bus 1 along the line connecting feasible points A and B given by

$$
\begin{aligned}
P_1(\mu) + jQ_1(\mu) &= (1-\mu)P_{A1} + \mu P_{B1} + j[(1-\mu)Q_{A1} + \mu Q_{B1}] \\
&= (1-\mu)\frac{V_m^2}{X}(-1+j) + \mu\frac{V_m^2}{X}(1+j) \\
&= \frac{jV_1(\mu)}{X}(V_1^*(\mu) - V_2^*(\mu))
\end{aligned}
\tag{4.15}
$$

Likewise for bus 2 injections, we obtain

$$
\begin{aligned}
P_2(\mu) + jQ_2(\mu) &= (1-\mu)P_{A2} + \mu P_{B2} + j[(1-\mu)Q_{A2} + \mu Q_{B2}] \\
&= (1-\mu)\frac{V_m^2}{X}(1+j) + \mu\frac{V_m^2}{X}(-1+j) \\
&= \frac{jV_2(\mu)}{X}(V_2^*(\mu) - V_1^*(\mu))
\end{aligned}
\tag{4.16}
$$

Some algebra yields the necessary voltage profile along the path of injections

$$
V_1(\mu) = V(\mu)
\tag{4.17}
$$

$$V_2(\mu) = V(\mu)e_j\theta(\mu) \tag{4.18}$$

where

$$V(\mu) = \frac{V_m}{\sqrt{2}}\sqrt{(2\mu - 1)^2 + 1} \tag{4.19}$$

$$\theta(\mu) = -\arctan\left(\frac{2(2\mu - 1)}{(2\mu - 1)^2 - 1}\right) \tag{4.20}$$

Note that θ varies from $\pi/2$ to $3\pi/2$ by a path that passes through π at $\mu = 0.5$. The minimum voltage magnitude along this path occurs at $\mu = 0.5$.

$$V_1(0.5) = \frac{V_m}{\sqrt{2}}, V_2(0.5) = -\frac{V_m}{\sqrt{2}} \tag{4.21}$$

Clearly at this point along the path of candidate injections, the minimum voltage constraint at one of the buses is violated. In fact, all of the injections along the path violate that minimum voltage constraint, except the endpoints. Therefore, the set of feasible power injections for this two-bus system is not convex. More complex power systems can be thought of as composed of two-bus subsystem. Therefore, the non-convex result applies to a very large class of power system models.

D.   Formulation of the Multi-Area OPF Problem

1.   Optimization Problem with Global Variables

The multi-area OPF determines, in a precise way, the active and reactive power that each generation unit in the system must generate. This is done to ensure that all demand and security constraints for the system are satisfied at a minimal cost for all interconnected areas. The resulting multi-area OPF problem is a large-scale non-convex optimization problem [23,58]. The general OPF problem can be reformulated as follows:

$$\min_{x,y_i}\sum_{i=1}^{N}F_i(x, y_i) \tag{4.22}$$

	x	y_1	y_2	y_3	y_4
$F_1...c_1$	▨	▨			
$F_2...c_2$	▨		▨		
$F_3...c_3$	▨			▨	
$F_4...c_4$	▨				▨

Fig. 14. FDT for four-element example OPGVs problem.

$$s.t. \quad c_i(x, y_i) \leq 0 \qquad\qquad (4.23)$$

where x is the a vector of variables on boundary buses, y_i is a vector of the ith area local variables. (4.22) is the objective function. (4.23) includes the equality and inequality constraints.

The Functional Dependence Table (FDT) is illustrated in Fig. 14. Similar to [59], I shade the (j, i)-entry of the table if the function of row j depends on the variables of column i. Throughout this Chapter, we use the FDT to illustrate the effect of the proposed problem transformation on the problem structure.

x is a vector of global variables, which is relevant to all systems, while, y_i is local to a single area. Note that while global variables appear in all of the constraints and objective function terms, local variables only appear in the objective function term and constraints corresponding to a single area. This problem falls under the category of non-convex Optimization Problems with Global Variables (OPGVs).

2. Formulation of the Decomposed OPGVs Problem

If the constraints in tie-lines are relaxed, the constraints in (4.23) will naturally belong to N different systems. Then global variables are needed to evaluate all of the constraints, whereas the local variables are needed only in the evaluation of the
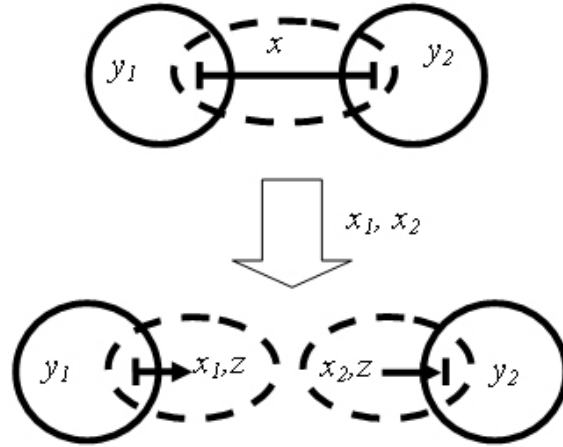
Fig. 15. Proposed decomposition scheme.

constraints belonging to one of the systems. Likewise, the objective function is the summation of N different terms, one per system; the local variables are only needed in the evaluation of one term. If the global variables are set to a fixed value, the problem breaks into N independent sub-problems. Decomposition algorithms use a so-called master problem to determine the global variables that are used by the sub-problems in order to find an OPGV minimizer. The proposed decomposition scheme is shown in Fig. 15.

First, a vector of target variables, z, is introduced. Then, a different vector x_i is used to represent the value of the global variables within each area. Compatibility constraints $(x_i = z)$ are introduced to force the global variables to take the same value, equal to the target variables, for all areas. The resulting problem is in the individual area.

$$\min_{z,x_i,y_i} \sum_{i=1}^{N} F_i(x_i, y_i) \tag{4.24}$$

$$s.t. \quad c_i(x_i, y_i) \leq 0, \quad i = 1 : N \tag{4.25}$$

$$h_i(x_i, z) = x_i - z = 0, \quad i = 1 : N \tag{4.26}$$

	z	x_1	y_1	x_2	y_2	x_3	y_3	x_4	y_4
h	■	■		■		■		■	
$F_1...c_1$		■	■						
$F_2...c_2$				■	■				
$F_3...c_3$						■	■		
$F_4...c_4$								■	■

Fig. 16. FDT for four-element example the modified OPGVs problem.

The FDT of the modified OPGVs problem is illustrated in Fig. 16, where separability of the local constraint sets can be observed, as well as non-separability of the introduced compatibility constraints.

Second, the quadratic penalty terms in the individual area's objective function are introduced to remove the compatibility constraints $x_i = z$ in (4.26).

$$\min_{z,x_i,y_i} \sum_{i=1}^{N} [F_i(x_i, y_i) + \gamma \|x_i - z\|_2^2]$$

$$s.t. \quad c_i(x_i, y_i) \leq 0, \quad i = 1 : N$$

(4.27)

where γ is the penalty parameter which must be used to weigh the quadratic penalty term $\|x_i - z\|_2^2$.

Finally, if the target variables are set to a fixed value, (4.27) breaks into N independent sub-problems. The sub-problem optimal-value functions can be used to formulate a master problem that only depends on the target variables.

The decentralized OPF computation architecture is presented Fig. 17. This is a two-level optimization model. *Master problem* is as follows:
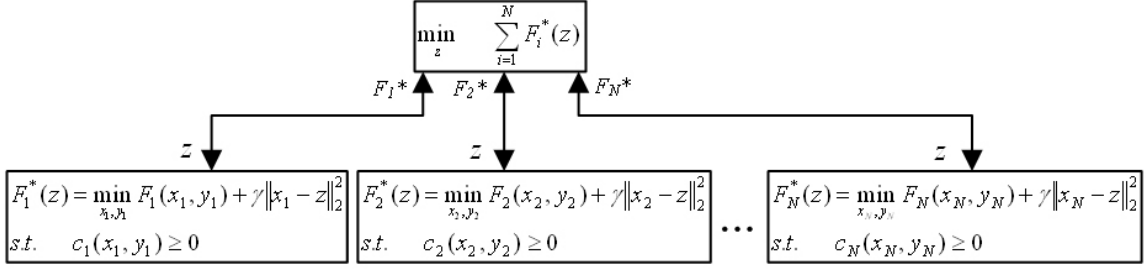
$$\min_{z} \sum_{i=1}^{N} F_i^*(z)$$

(4.28)

Fig. 17. Computation architecture for the proposed decomposition method.

Sub-problem will then be written as follows:

$$F_i^*(z) = \min_{x_i, y_i}[F_i(x_i, y_i) + \gamma \|x_i - z\|_2^2]$$

$$s.t. \quad c_i(x_i, y_i) \leq 0, \quad i = 1 : N$$

(4.29)

The FDT of the relaxed problem is illustrated in Fig. 18, where the desired full separability of the sub-problem function can be clearly observed.

E. Decentralized OPF Algorithm

The proposed algorithm assumes that areas do not share their network data and economic information; however they are willing to cooperate via a central coordinator for system wide computations. The function of each area is to calculate its local optimal objective function and its gradient. The function of central coordinator is to collect local optimal objective functions and their gradients from areas, and then optimize and update global variables.

1. Central Coordinator Level

The central coordinator is to solve the master problem which is an unconstrained optimization problem and can be solved by basic BFGS quasi-Newton unconstrained optimization algorithm. The algorithm is as follow:

Fig. 18. FDT for four-element example relaxted OPGVs problem with full separable constraint sets in sub-problem

Step 1: Initialization; Initialize the penalty parameter γ, the quasi-Newton Hessian approximation $B = I$, and the optimality tolerance $\epsilon = 1 \times 10_{-5}$.

Step 2: Choose a starting point z_0 and set $z = z_0$; Call sub-problem with γ to evaluate the objective function F^* and its gradient ∇F^*.

Step 3:

While$(\|\nabla F^*(z)\|/|1 + F^*(z)| < \epsilon)$

Step 3.1 Search directions. Solve $B \triangle z = -\nabla F^*(z)$,

Step 3.2 Line search: Set $\alpha = 1$

While$(F^*(z + \triangle z) - F^*(z)) > \sigma \bigtriangledown F^*(z) \triangle z$

Set $\alpha = \alpha/2$, Call **sub-problem** to evaluate the objective function F^* and its gradient $\bigtriangledown F^*$.

Endwhile

$s = \alpha \triangle z$, $y = \bigtriangledown F^*(z + \alpha \triangle z)$

$z = z + s$, update $F^*(z)$ and $\bigtriangledown F^*(z)$.

Step 3.3 BFGS update

$$B = B - \frac{Bss^T B}{s^T Bs} + \frac{yy^T}{y^T s}$$

Endwhile

Step 4:

if $\sum_{i=1}^{N} \|x_i - z\|_2^2/(1 + \|z\|) < \epsilon$, then stop

Else increase γ which is drive the smaller $\sum_{i=1}^{N} \|x_i - z\|_2^2/(1 + \|z\|) < \epsilon$, Call **sub-problem** with γ to evaluate the objective function F^* and its gradient ∇F^*; Go to **Step 3**.

Endif

Note that the master problem's objective function and gradient can be evaluated at sub-problem solutions as:

$$F^*(z) = \sum_{i=1}^{N} F_i^*(z) \tag{4.30}$$

$$\nabla F^*(z) = -2\gamma \sum_{i=1}^{N} (x_i^* - z) \tag{4.31}$$

2. Local Level

The proposed method decomposes the original integrated OPF problem into several smaller size subproblem which are solved independently. The sub-problem (4.29) is a modified traditional OPF problem. The penalty part $\gamma\|x_i - z\|_2^2$ will be added into the objective function of the OPF model. This constrained optimization problem can be solved by the sequential quadratic programming or linear programming algorithms, which are commonly used by most OPF programs.

Each area builds an OPF model with the operating and economic information within itself. The tie-line power flows are considered as injections of boundary buses which can be calculated from the target global variables z. The local slack bus for each area except the one with the global slack bus will be updated during the each communication between the central and local level. If the local slack bus is on the boundary of the area, the phase angle is automatically updated by the master problem.

In Fig. 19, the solution algorithm presented in this chapter is illustrated. The

Table XII. Coefficients for generation cost polynomial

	$c_0(\$)$	$c_1(\$/MW)$	$c_2(\$/MW^2)$
Gen1	0	2	0.02
Gen2	0	1.75	0.0175
Gen22	0	1	0.0625
Gen27	0	3.25	0.00834
Gen23	0	3	0.025
Gen13	0	3	0.025

figure show two main parts of this algorithm: 1) coordination through the penalty updates (outer loop) and the solution of the master problem (inner loop), and 2) distributed optimization by solving the sub-problems. For the outer loop, the converge criteria is that the maximal consistency constraint violation must be smaller than tolerance $\sum_{i=1}^{N} \|x_i - z\|_2^2/(1 + \|z\|) < \epsilon$. The converge criteria for the inner loop is set as: $\|\nabla F^*(z)\|/|1 + F^*(z)| < \epsilon$.

F. Numerical Results

The proposed decomposition method for multi-area OPF problem is tested on IEEE 30 bus system. The system is divided into three areas as shown in Fig. 20. The network data and line, voltage, generation limits can be found at MATPOWER [60]. Here, we just consider the cost for active power produced by the corresponding generators, which is expressed as a polynomial $Gencostt = c_0 + c_1 * P + c_2 * P^2$. The coefficients c_0, c_1 and c_2 are given in Table XII.

fmincon.m and *fminunc.m* found in Matlab's Optimization Toolbox 2.0 or later are used to solve the modified constrained and unconstrained OPF models at the local and central coordinator levels, respectively. In this case study, there are 22 global variables which are the boundary bus voltage magnitudes and angles. The master and
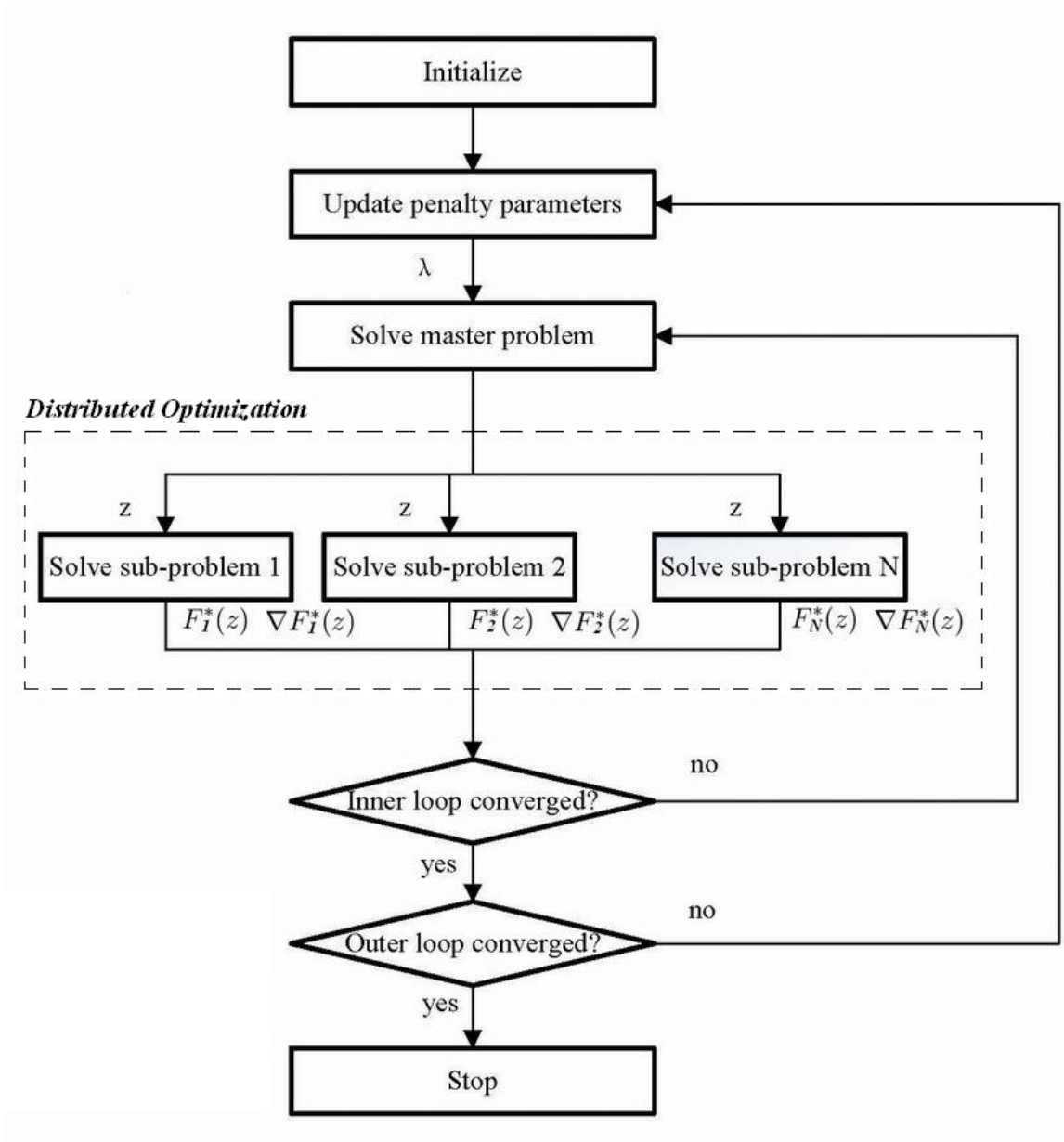
Fig. 19. Illustration of proposed solution algorithm.
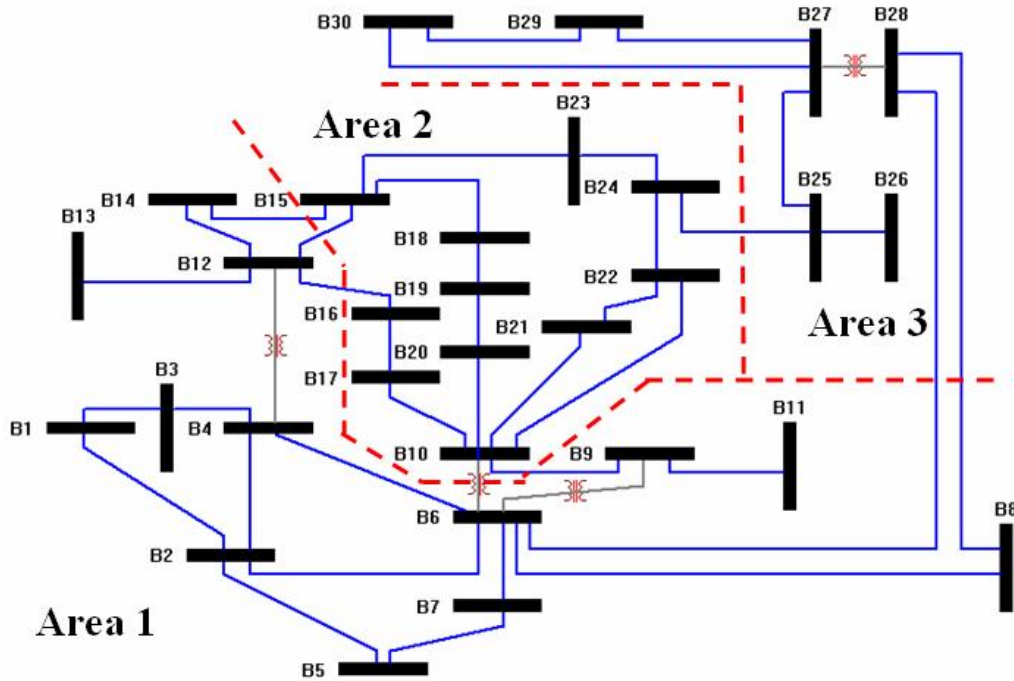
Fig. 20. IEEE 30-bus partitioned interconnected system.

sub problem optimal-value functions are shown in Fig. 21, where nsub is the number of sub-problems that have to be solved in order to find the overall minimizer.

In order to compare the numerical performance and accuracy, OPF solver in MATPOWER is used to calculate the minimum cost of generation in the integrated system.

The numerical performance of the decomposition algorithm is compared with that of the integrated OPF solver in Table XIII. For the decomposition method, the first row shows the number of iterations required to solve the master problem; the second row gives the number of sub-problems that have to be solved in order to find the overall minimizer; this quantity provides a measure for the amount of communication required between the master problem and the sub-problems; the third row contains the average number of function evaluations needed to solve each sub-problem. In
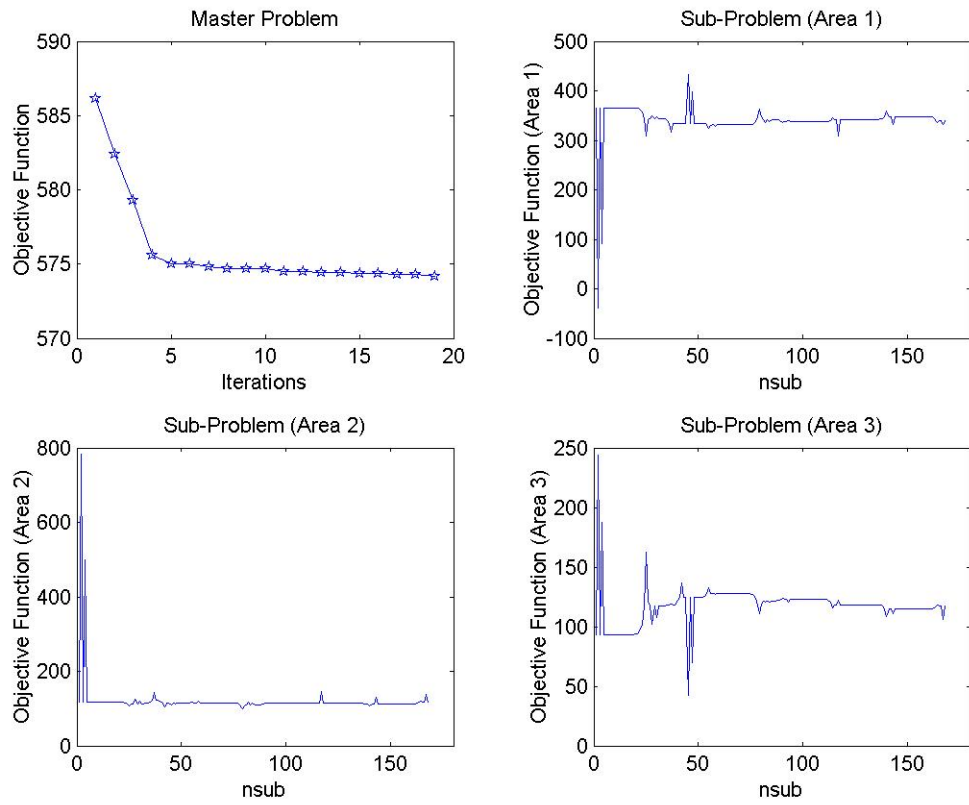
Fig. 21. Master and sub problem optimal-value functions.

Table XIII. Numerical result

	Decentralized OPF result	Traditional OPF result
Ite	19	22
nsub	168	
feval	13	59

Table XIV. Comparison of the minimum generation cost by decentralized and traditional OPF methods

	Decentralized OPF result ($/hr)	Traditional OPF result ($/hr)
Objective	574.14	574.52

the integrated OPF method, the third row shows the number of function evaluations needed to solve for the overall optimization problem. The proposed decomposition method requires more computations compared to the integrated method in order to overcome the data deficiency.

The accuracy comparison between the integrated and the decomposition methods can be seen in Table XIV and Table XV. Table XIV and Table XV list the objective

Table XV. Coefficients for generation cost polynomial

	Decentralized OPF result (MW)	Traditional OPF result (MW)
Gen1	43.31	43.79
Gen2	57.39	57.96
Gen22	23.38	23.07
Gen27	33.21	32.63
Gen23	17.5	16.81
Gen13	16.72	17.35

function and the detailed generator active power output computed by decentralized or traditional OPF method, respectively. The results of these two solutions are very close, yielding an acceptable approximation. These results strongly imply that the proposed method effectively overcomes the data deficiency for the multi-area OPF problem.

G. Conclusion

A decomposition method for decentralized OPF problem in a large interconnected multi-area power system is proposed. The method assumes that areas do not share their network data among themselves; however they are willing to cooperate via a central coordinator.

The proposed decomposition algorithm allows collaboration of different areas to find their optimal solutions while exchanging limited amount of data and information among them. Typically each area must rely on complex operating and economic information. Such information can not be practically exported to a specific area, not to mention the difficulties associated with its incorporation into the integrated solution. Hence, the proposed approach will serve a useful and essential purpose under such circumstances. Proposed method is validated by simulations which are carried out on the IEEE 30-bus system using traditional OPF and the proposed decentralized OPF methods.

CHAPTER V

CONCLUSIONS

A. Summary

In the emerging competitive environment, TTC and economic dispatch are very important functions of independent system operators (ISOs), which are required to ensure the delivery of all the transactions without any violation on the operating limits of a transmission system. Operators are facing the needs to monitor and coordinate power transactions taking place over long distance in different areas. Areas are reluctant to share network operating and economic information between them, while they are willing to cooperate via a central coordinator for system wide analysis. This dissertation proposes three different decomposition algorithms for multi-area TTC and economic dispatch studies.

A decomposition algorithm based on Power Transfer Distribution Factors (PTDFs) for multi-area TTC computation is proposed in Chapter II. The variations of PTDFs with operating point are approximated by a quadratic equation and then are applied to area's TTC calculation by Repeated Power Flow (RPF), while a central entity co-ordinates these results to determine the final system-wide TTC value. The behavior of PTDFs near static collapse point is discussed and demonstrates that the proposed algorithm can be applied only to TTC studies without the consideration of voltage stability problems.

Chapter III initiates a network decomposition algorithm based on REI-type net-work equivalents. REI-type equivalents and Continuation Power Flow (CPF) tech-niques are introduced in this chapter. A two-level computation architecture is pro-posed: each area uses REI equivalents of external areas to compute its TTC via

the CPF, the central entity coordinators distribute the equivalents from areas and compare the tie-line information. The selection and updating procedure for the continuation parameter employed by the CPF are implemented in a distributed but coordinated manner. The computation in this chapter takes into account the limits on the line flows, bus voltage magnitude, generator reactive power, voltage stability and the loss of line contingencies.

Chapter IV introduces an Inexact Penalty Decomposition algorithm developed by Operation & Research scholars into Optimal Power Flow (OPF) problem in power system. The traditional OPF problem with voltage constraints is demonstrated as a non-convex optimization problem and the boundary variables in the traditional OPF problem are considered as global variables. Thus, the original OPF problem is treated as an optimization problem with global variables. Quadratic penalty functions are used to relax the compatible constraints between the global variables and the local variables. The solution is proposed to be implemented by using a two-level computational architecture.

The advantages in the use of decomposition are both computational and organizational. From a computational perspective, the sub-problems are usually easier to solve than the original problem. The sub-problems are, by definition, smaller than the original problems. Moreover, the sub-problem might have special properties, which enable the use of efficient specialized algorithms. Furthermore, decomposition algorithms are naturally suited for implementation on machines with parallel architecture. From an organizational perspective, decomposition algorithms allow the different areas collaborating on a project to find the final result while keeping the amount of communication required between them limited. Typically, each area must rely on complex operating and economic information. Porting all the information to a specific area is judged to be impractical (sometimes some information

is not available). Also it would raise the issue of how local information would be incorporated into the integrated system. Under such circumstances decomposition algorithms become essential. In this dissertation I propose three novel decomposition frameworks. Decentralized versions of power flow methods for multi-area power system are also presented based on the decomposition frameworks. For further practical use, information exchange and coordination across multiple areas are discussed.

B.   Future Work

The research is not finished. In the future, my research in this dissertation can be improved in the following aspects.

First, this dissertation is mainly focused on the TTC study. Available Transfer Capability (ATC) is another important index for operation and planning in ISO. I plan to extend the multi-area TTC scheme to evaluate the ATC study, which involves other functions such as Capability Benefit Margin (CBM), and Transfer Reliability Margin (TRM).

Second, contingencies may be considered in the algorithm proposed in Chapter II. Also, the simultaneous transfer may be studied in the algorithm proposed in Chapter III.

Third, the decomposition algorithm in Chapter IV is suitable for general OPF problem. The inter-regional coordination that allows separate control while remaining a seamless market become a critical aspect in market design. Therefore, this algorithm can be used to deal with the issues of inter-market congestion management.

Fourth, the decomposition algorithm in Chapter IV is proposed for the non-convex optimization problem and costs a lot of computation time for the communication between master and local problems. If I release the voltage magnitude in

OPF problem, the direct method of multipliers is a way to save computation time in communication.

REFERENCES

[1] "Available transfer capability definitions and determination," Tech. Rep., North American Electric Reliability Council, Princeton, NJ, 1996.

[2] I. Dobson, S. Greene, R. Rajaraman, C.L. Demarco, F.L. Alvarado, M. Glavic, J. Zhang, and R. Zimmerman, "Electrical power transfer capability: Concepts, applications, sensitivity, uncertainty," Project Report, Power Systems Engineering Research Center, 2001.

[3] FERC, "United States of America 112 ferc ¶61,353," *[Online] elibrary.ferc.gov/idmws/common/opennat.asp?fileID=10828077*, September 2005.

[4] G.L. Landgren, H.L. Terhune, and R.K. Angel, "Transmission interchange capability - analysis by computer," *IEEE Transactions on Power Apparatus and Systems*, vol. 91, no. 6, pp. 2405–2414, May 1972.

[5] G.C. Ejebe, J.G. Waight, M. Santos-Nieto, and W.F. Tinney, "Fast calculations of linear available transfer capability," in *Proc. Power Industry Computer Applications Conf.*, 1999, pp. 255–260.

[6] R.D. Christie, B.F. Wollenberg, and I. Wangersteen, "Transmission management in the deregulated environment," *Proc. IEEE*, vol. 88, no. 2, pp. 170–195, February 2000.

[7] B. Gao, G.K. Morison, and P. Kundur, "Towards the development of a systematic approach for voltage stability assessment of large-scale power system," *IEEE Transactions on Power Systems*, vol. 11, no. 3, pp. 1314–1324, August 1996.

[8] G.C. Ejebe, J. Tong, G.C. Waight, J.G. Frame, X. Wang, and W.F. Tinney, "Available transfer capability calculations," *IEEE Transactions on Power Systems*, vol. 13, no. 4, pp. 1521–1527, November 1998.

[9] V. Ajjarapu and C. Christy, "The continuation power flow: A tool for steady state voltage stability analysis," *IEEE Transactions on Power Systems*, vol. 7, no. 1, pp. 416–423, February 1992.

[10] C.A. Canizares and F.L. Alvarado, "Point of collapse and continuation methods for large acdc systems," *IEEE Transactions on Power Systems*, vol. 8, no. 1, pp. 1–8, February 1993.

[11] H.S. Chiang, A.J. Flueck, K.S. Shah, and N. Balu, "Cpflow: A practical tool for tracing power system steady-state stationary behavior due to load and generation variations," *IEEE Transactions on Power Systems*, vol. 10, no. 2, pp. 623–634, May 1995.

[12] H.W. Dommel and W.F. Tinney, "Optimal power flow solutions," *IEEE Transactions on Power Apparatus and Systems*, vol. 87, no. 10, pp. 1866–1876, 1968.

[13] J.A. Momoh, M.E. El-Hawary, and R. Adapa, "A review of selected optimal power flow literature to 1993 part ii: Newton, linear programming and interior point methods," *IEEE Transactions on Power Systems*, vol. 14, no. 1, pp. 105–111, February 1999.

[14] P. Bresesti, D. Lucarella, P. Marannino, R. Vailati, and F. Zanellini, "An opf-based procedure for fast ttc analyses," in *Proc. Power Eng. Soc. General Meeting*, 2002, vol. 3, pp. 1504–1509.

[15] Y. Ou and C. Singh, "Assessment of available transfer capability and margins," *IEEE Transactions on Power Systems*, vol. 17, no. 2, pp. 463–468, May 2002.

[16] FERC, "Order no.2000, regional transmission organization (rto)- final rule," *[Online] http://www.ferc.gov/legal/maj-ord-reg/land-docs/RM99-2A.pdf*, December 1999.

[17] European Transmission System Operators (ETSO), "Evaluation of congestion management methods for cross-border transmission," *[Online] http://www.etso-net.org*, November 1999.

[18] Powertech Labs Inc, "Dynamic security assessment (DSA) tools version 6.0," *[Online] http://www.dsapowertools.com*, May 2006.

[19] V&R Energy Inc, "Physical and operational margins (POM) version 3.0," *[Online] http://www.vrenergy.com*, 2005.

[20] L. Zhao and A. Abur, "Two-layer multi-area total transfer capability computation," in *Proc. IREP Symp.*, Cortina D'Ampezzo, Italy, August 23-27 2004.

[21] T. Stoilov and K. Stoilova, *Noniterative Coordination in Multilevel Systems*, pp. 1–56, Norwell, MA: Kluwer Acdemic Publishers, 1999.

[22] M. Shaaban, W. Li, H. Liu, Z. Yan, Y. Ni, and F. Wu, "Atc calculation with steady-state security constraints using benders decomposition," in *IEE Proc. on Generation, Transmission and Distributio*, September 2003, vol. 150, pp. 611–615.

[23] A. Wood and B. Wollenberg, *Power Generation Operation and Control*, New York: Wiley, 2th edition, 1996.

[24] R. Baldick, "Variation of distribution factors with loading," *IEEE Transactions on Power Systems*, vol. 18, no. 4, pp. 1316–1323, November 2003.

[25] S. Grijalva, "Complex flow-based nonlinear ATC screening," Ph.D. dissertation, Univ. Illinois at Urbana-Champaign, Urbana, IL, July 2002.

[26] A. Fradi, S. Brignone, and B. F. Wollenberg, "Calculation of energy transaction allocation factors," *IEEE Transactions on Power Systems*, vol. 16, no. 2, pp. 266–272, May 2001.

[27] T.V. Cutsem, "Voltage instability: Phoenomena, countermeasures, and analysis methods," *Proceedings of the IEEE*, vol. 88, no. 2, pp. 208–227, February 2000.

[28] "Suggested techniques for voltage stability analysis," Tech. Rep., IEEE Working Group on Voltage Stability, IEEE Publication 93TH0620-5PWR, 1993.

[29] T.V. Cutsem, Y. Jacquemart, J.-N. Marquet, and P. Pruvot, "Extensions and applications of a mid-term voltage stability analysis method," in *Bulk Power System Phenomena II - Voltage Stability and Security*, Davos, Switzerland, 1994, pp. 251–270.

[30] T.V. Cutsem, Y. Jacquemart, J.-N. Marquet, and P. Pruvot, "A comprehensive analysis of mid-term voltage stability," *IEEE Transactions on Power Systems*, vol. 10, no. 3, pp. 1173–1182, August 1995.

[31] CIGRE Report, "Planning against voltage collapse," *Electra*, vol. 111, pp. 55–75, 1987.

[32] Y. Mansour, C.D. James, and D.N. Pettet, "Voltage stability and security," in *Bulk Power System Phenomena II - Voltage Stability and Security*, Potosi, MO, September 19-24 1988, pp. 2.9–2.25.

[33] T.V. Cutsem, "A method to compute reactive power margins with respect to voltage collapse," *IEEE Transactions on Power Systems*, vol. 6, no. 1, pp. 145–156, Feburary 1991.

[34] O.O. Obadona and G.J. Berg, "Determination of voltage stability limit in multimachine power systems," *IEEE Transactions on Power Systems*, vol. 3, no. 4, pp. 1545–1554, November 1988.

[35] C.J. Parker, I.F. Morrison, and D. Sutanto, "Application of an optimization method for determining the reactive maring from voltage collapse in reactive power planning," *IEEE Transactions on Power Systems*, vol. 11, no. 4, pp. 1473–1481, November 1996.

[36] G.D. Irisarri, X. Wang, J. Tong, and S. Mokhtari, "Maximum loadability of power systems using interior point non-linear optimization method," *IEEE Transactions on Power Systems*, vol. 12, no. 1, pp. 162–172, Feburary 1997.

[37] L. Min, A. Abur, and L. Zhao, "Two-level multi-area TTC calculation by updating power transfer distribution factors," in *Proc. Power Eng. Soc. General Meeting*, San Francisco, CA, June 12-16 2005.

[38] B.H. Kim and R. Baldick, "Coarse-grained distributed optimal power flow," *IEEE Transactions on Power Systems*, vol. 12, no. 2, pp. 932–939, May 1997.

[39] X. Wang, Y.H. Song, and Q. Lu, "Lagrangian decomposition approach to active power congestion management across interconnected regions," *Proc. Inst. Elect. Eng., Gen., Transm., Distrib.*, vol. 148, no. 5, pp. 497–503, September 2001.

[40] P.N. Biskas and A.G. Bakirtzis, "Decentralised congestion management of interconnected power systems," *Proc. Inst. Elect. Eng., Gen., Transm., Distrib.*,

vol. 149, no. 4, pp. 432–438, July 2002.

[41] S.M. Deckman, A. Pizzolante, A. Monticelli, B. Scott, and O. Alsac, "Studies on power system load flow equivalencing," *IEEE Transactions on Power Apparatus and Systems*, vol. 99, pp. 2301–2310, November 1980.

[42] P. Dimo, *Nodal Analysis of Power System*, Turibrige Wells, Kent, U.K.: Abacus Press, 1975.

[43] W.F. Tinney and W.L. Powell, "The REI approach to power network equivalents," in *Transl.: 1977 PICA Conf.*, Toronto, ON, Canada, May 1977, pp. 312–320.

[44] S.C. Savulescu, "Equivalents for security analysis of power system," *IEEE Transactions on Power Apparatus and Systems*, vol. 100, pp. 2672–2682, May 1981.

[45] T.E. Dyliacco, S.C. Savulescu, and K.A. Ramarao, "An on-line topological equivalent of a power system," *IEEE Transactions on Power Apparatus and Systems*, vol. 97, pp. 1550–1563, Sep./Oct. 1978.

[46] J.F. Dopazo, G. Irisarri, and A.M. Sasson, "Real-time external system equivalent for online contigency analysis," *IEEE Transactions on Power Apparatus and Systems*, vol. 98, pp. 2153–2171, November 1979.

[47] J.D. Weber, T.J. Overbye, and C.L. DeMarco, "Inclusion of price dependent load models in the optimal power flow," in *Proc. of 31st Hawaii International Conference on System Sciences.*, Kona, HI, January 1998, pp. 62–70.

[48] "Optimal power flow: solution techniques, requirements, and challenges," *IEEE Tutorial Course*, 1996.

[49] "Virtual regional transmission organizations, the standard market design, a conceptual development with illustrative examples," Tech. Rep., Electric Power Research Institute, Palo Alto, CA, 2003.

[50] J. A. Aguado, V. H. Quintana, and A. J. Conejo, "Optimal power flows of interconnected power systems," in *Proc. of the IEEE Power Engineering Society Summer Meeting.*, Kona, HI, 1999, vol. 2, pp. 814–819.

[51] A.J. Conejo and J.A. Aguado, "Optimal power flows of interconnected power systems," *IEEE Transactions on Power Systems*, vol. 13, no. 4, pp. 1272–1278, November 1998.

[52] R. Baldick, B.H. Kim, C. Chase, and Y. Luo, "A fast distributed implementation of optimal power flow," *IEEE Transactions on Power Systems*, vol. 14, no. 3, pp. 858–864, August 1999.

[53] A. Demiguel, "Two decomposition algorithms for non-convex optimization problems with global variables," Ph.D. dissertation, Stanford University, Palo Alto, CA, 2001.

[54] W. Hogan, "Contract networks for electric power transmission: technical reference," *[Online] http://ksghome.harvard.edu/ whogan/acnetref/pdf*, 1992.

[55] H.P. Chao and S. Peck, "An market mechanism for electric power transmission," *J. Regulatory Econ.*, vol. 10, pp. 25–59, July 1996.

[56] B.C. Lesieutre and I.A. Hiskens, "Convexity of the set of feasible injection and revenue adequacy in ftr market," *IEEE Transactions on Power Systems*, vol. 20, no. 4, pp. 1790–1797, November 2005.

[57] S. Oren and A. Ross, "Economic congestion relief across multiple regions requires tradable physical flow-gate rights," *IEEE Transactions on Power Systems*, vol. 17, no. 1, pp. 159–165, Feburary 2002.

[58] M. Huneault and F.D. Galiana, "A survey of the optimal power flow literature," *IEEE Transactions on Power Systems*, vol. 6, no. 2, pp. 762–770, May 1991.

[59] T.C. Wagner, "A general decomposition methodology for optimal system design," Ph.D. dissertation, University of Michigan, Ann Arbor, MI, 1993.

[60] "Matpower v3.1b1 manual," *[Online] http://www.pserc.cornell.edu/matpower/*, August 2006.

APPENDIX A

HIGH-ORDER DERIVATIVES OF THE PTDFS

The second-order derivatives of the active power flow of line jk with respect to the state variables can be expressed as:

$$
\begin{bmatrix} \dfrac{\partial^2 P_{jk}}{\partial \theta_i^2} \\ \dfrac{\partial^2 P_{jk}}{\partial V_i^2} \end{bmatrix} = \begin{bmatrix} \dfrac{\partial^2 P_m}{\partial \theta_i^2} & \dfrac{\partial^2 Q_m}{\partial \theta_i^2} \\ \dfrac{\partial^2 P_m}{\partial V_i^2} & \dfrac{\partial^2 Q_m}{\partial V_i^2} \end{bmatrix} \begin{bmatrix} \dfrac{\partial P_{jk}}{\partial P_m} \\ \dfrac{\partial P_{jk}}{\partial Q_m} \end{bmatrix} + \begin{bmatrix} (\dfrac{\partial P_m}{\partial \theta_i})^2 & (\dfrac{\partial Q_m}{\partial \theta_i})^2 \\ (\dfrac{\partial P_m}{\partial V_i})^2 & (\dfrac{\partial Q_m}{\partial V_i})^2 \end{bmatrix} \begin{bmatrix} \dfrac{\partial^2 P_{jk}}{\partial P_m^2} \\ \dfrac{\partial^2 P_{jk}}{\partial Q_m^2} \end{bmatrix}
$$

$$(A.1)$$

Thus, the first-order derivative of the PTDFs with respect to the injection at bus m can be expressed as:

$$
\begin{bmatrix} \dfrac{\partial^2 P_{jk}}{\partial P_m^2} \\ \dfrac{\partial^2 P_{jk}}{\partial Q_m^2} \end{bmatrix} = \begin{bmatrix} (\dfrac{\partial P_m}{\partial \theta_i})^2 & (\dfrac{\partial Q_m}{\partial \theta_i})^2 \\ (\dfrac{\partial P_m}{\partial V_i})^2 & (\dfrac{\partial Q_m}{\partial V_i})^2 \end{bmatrix}^{-1} \left\{ \begin{bmatrix} \dfrac{\partial^2 P_{jk}}{\partial \theta_i^2} \\ \dfrac{\partial^2 P_{jk}}{\partial V_i^2} \end{bmatrix} - \begin{bmatrix} \dfrac{\partial^2 P_m}{\partial \theta_i^2} & \dfrac{\partial^2 Q_m}{\partial \theta_i^2} \\ \dfrac{\partial^2 P_m}{\partial V_i^2} & \dfrac{\partial^2 Q_m}{\partial V_i^2} \end{bmatrix} \begin{bmatrix} \dfrac{\partial P_{jk}}{\partial P_m} \\ \dfrac{\partial P_{jk}}{\partial Q_m} \end{bmatrix} \right\}
$$

$$(A.2)$$

where, the elements in $\left[\dfrac{\partial^2 P_{jk}}{\partial P_i^2}, \dfrac{\partial^2 P_{jk}}{\partial Q_i^2} \right]^T$ can be obtained from (2.28). The elements in $\left[\dfrac{\partial P_{jk}}{\partial P_m}, \dfrac{\partial P_{jk}}{\partial Q_m} \right]^T$ are shown in (2.30). Elements of other matrices on the right hand side of (A.2) can be obtained from power flow equation.

The third-order derivatives of the active power flows of line jk with respect to

the state variables can be expressed as:

$$
\begin{bmatrix} \dfrac{\partial^3 P_{jk}}{\partial \theta_i^3} \\ \dfrac{\partial^3 P_{jk}}{\partial V_i^3} \end{bmatrix} = \begin{bmatrix} \dfrac{\partial^3 P_m}{\partial \theta_i^3} & \dfrac{\partial^3 Q_m}{\partial \theta_i^3} \\ \dfrac{\partial^3 P_m}{\partial V_i^3} & \dfrac{\partial^3 Q_m}{\partial V_i^3} \end{bmatrix} \begin{bmatrix} \dfrac{\partial P_{jk}}{\partial P_m} \\ \dfrac{\partial P_{jk}}{\partial Q_m} \end{bmatrix} + \begin{bmatrix} (\dfrac{\partial P_m}{\partial \theta_i})^3 & (\dfrac{\partial Q_m}{\partial \theta_i})^3 \\ (\dfrac{\partial P_m}{\partial V_i})^3 & (\dfrac{\partial Q_m}{\partial V_i})^3 \end{bmatrix} \begin{bmatrix} \dfrac{\partial^3 P_{jk}}{\partial P_m^3} \\ \dfrac{\partial^3 P_{jk}}{\partial Q_m^3} \end{bmatrix}
$$

$$
+ 3 \cdot \begin{bmatrix} \dfrac{\partial^2 P_m}{\partial \theta_i^2}\dfrac{\partial P_m}{\partial \theta_i} & \dfrac{\partial^2 Q_m}{\partial \theta_i^2}\dfrac{\partial Q_m}{\partial \theta_i} \\ \dfrac{\partial^2 P_m}{\partial V_i^2}\dfrac{\partial P_m}{\partial V_i} & \dfrac{\partial^2 Q_m}{\partial V_i^2}\dfrac{\partial Q_m}{\partial V_i} \end{bmatrix} \begin{bmatrix} \dfrac{\partial^2 P_{jk}}{\partial P_m^2} \\ \dfrac{\partial^2 P_{jk}}{\partial Q_m^2} \end{bmatrix}
$$

$$(A.3)$$

Thus, the second-order derivatives of the PTDFs with respect to the injection at bus m can be expressed as:

$$
\begin{bmatrix} \dfrac{\partial^3 P_{jk}}{\partial P_m^3} \\ \dfrac{\partial^3 P_{jk}}{\partial Q_m^3} \end{bmatrix} = \begin{bmatrix} (\dfrac{\partial P_m}{\partial \theta_i})^3 & (\dfrac{\partial Q_m}{\partial \theta_i})^3 \\ (\dfrac{\partial P_m}{\partial V_i})^3 & (\dfrac{\partial Q_m}{\partial V_i})^3 \end{bmatrix}^{-1} \left\{ \begin{bmatrix} \dfrac{\partial^3 P_{jk}}{\partial \theta_i^3} \\ \dfrac{\partial^3 P_{jk}}{\partial V_i^3} \end{bmatrix} - \begin{bmatrix} \dfrac{\partial^3 P_m}{\partial \theta_i^3} & \dfrac{\partial^3 Q_m}{\partial \theta_i^3} \\ \dfrac{\partial^3 P_m}{\partial V_i^3} & \dfrac{\partial^3 Q_m}{\partial V_i^3} \end{bmatrix} \begin{bmatrix} \dfrac{\partial P_{jk}}{\partial P_m} \\ \dfrac{\partial P_{jk}}{\partial Q_m} \end{bmatrix} \right.
$$

$$
\left. - 3 \cdot \begin{bmatrix} \dfrac{\partial^2 P_m}{\partial \theta_i^2}\dfrac{\partial P_m}{\partial \theta_i} & \dfrac{\partial^2 Q_m}{\partial \theta_i^2}\dfrac{\partial Q_m}{\partial \theta_i} \\ \dfrac{\partial^2 P_m}{\partial V_i^2}\dfrac{\partial P_m}{\partial V_i} & \dfrac{\partial^2 Q_m}{\partial V_i^2}\dfrac{\partial Q_m}{\partial V_i} \end{bmatrix} \begin{bmatrix} \dfrac{\partial^2 P_{jk}}{\partial P_m^2} \\ \dfrac{\partial^2 P_{jk}}{\partial Q_m^2} \end{bmatrix} \right\}
$$

$$(A.4)$$

where, the elements in $\left[\dfrac{\partial^3 P_{jk}}{\partial P_i^3}, \dfrac{\partial^3 P_{jk}}{\partial Q_i^3} \right]^T$ can be obtained from (2.28). The elements in $\left[\dfrac{\partial^2 P_{jk}}{\partial P_m^2}, \dfrac{\partial^2 P_{jk}}{\partial Q_m^2} \right]^T$ are shown in (A.2). Elements of other matrices on the right hand side of (A.4) can be obtained from power flow equation.

VITA

Liang Min was born in Huzhou, Zhejiang, China. He received his BS and MS degrees in Electrical Engineering from Tianjin University, Tianjin, China in 2001 and 2004, respectively. In August 2004, he began pursuing his Ph.D. degree in the Department of Electrical Engineering at Texas A&M University and graduated in May 2007. He has been a research assistant for his advisor, Dr. Ali Abur. He can be reached at:

Liang Min

17-102 Hongfeng Xincun

Huzhou, Zhejiang 313000

China

The typist for this dissertation was Liang Min.